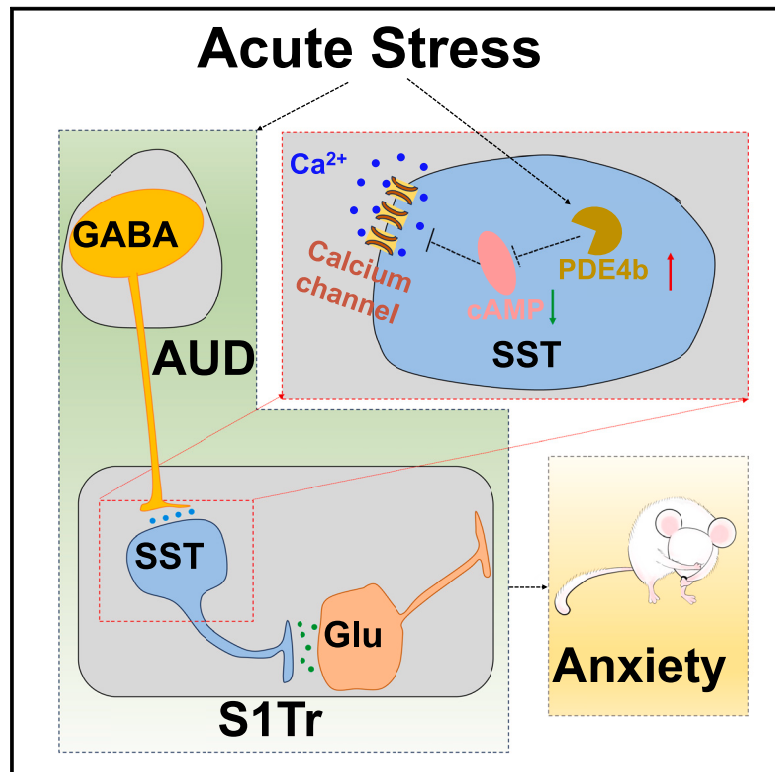


Pde4b-regulated cAMP signaling pathway in the AUD^{GABA}-S1Tr^{Sst} circuit underlies acute-stress-induced anxiety-like behavior

Graphical abstract



Authors

Zhi-Xin Xiao, Xiao-Ya Wang, Nan Zhou, ..., Xia Zhang, Hua-Min Xu, Xu-Feng Xu

Correspondence

xia.zhang@qdu.edu.cn (X.Z.),
huaminxu@qdu.edu.cn (H.-M.X.),
xuxufeng@qdu.edu.cn (X.-F.X.)

In brief

Xiao et al. demonstrate that acute stress elevates the expression of Pde4b protein in S1Tr^{Sst} neurons' inputs from AUD^{GABA}, which leads to excessive degradation of cAMP, resulting in a hypoactivity of S1Tr^{Sst} neurons during subsequent behavioral tests, thus producing anxiety.

Highlights

- Acute stress induces the activation and desensitization of S1Tr^{Sst} neurons
- S1Tr^{Sst} neurons are necessary and sufficient to regulate acute-stress-induced anxiety
- AUD^{GABA}-S1Tr^{Sst} pathway controls acute-stress-induced anxiety
- Knockout of Pde4b in AUD^{GABA}-S1Tr^{Sst} neural circuit reduces acute-stress-elicited anxiety



Article

Pde4b-regulated cAMP signaling pathway in the AUD^{GABA}-S1Tr^{Sst} circuit underlies acute-stress-induced anxiety-like behavior

Zhi-Xin Xiao,^{1,4} Xiao-Ya Wang,^{1,4} Nan Zhou,^{2,4} Xue-Tong Yi,¹ Xiao-Qi Zhang,¹ Qi-Lin Wu,¹ Zhuo Li,¹ Xia Zhang,^{1,3,*} Hua-Min Xu,^{1,*} and Xu-Feng Xu^{1,5,*}

¹School of Basic Medicine, The Affiliated Hospital of Qingdao University, Qingdao University, Qingdao 266000, China

²Department of Urology, Qilu Hospital of Shandong University, Jinan 250012, China

³Department of Neurology, West China Hospital of Sichuan University, Chengdu 610041, China

⁴These authors contributed equally

⁵Lead contact

*Correspondence: xia.zhang@qdu.edu.cn (X.Z.), huaminxu@qdu.edu.cn (H.-M.X.), xuxufeng@qdu.edu.cn (X.-F.X.)

<https://doi.org/10.1016/j.celrep.2025.115253>

SUMMARY

Acute-stress-induced anxiety helps animals avoid danger, but the neural and molecular mechanisms controlling this behavior remain largely elusive. Here, we find that acute physical stress activates many neurons in the primary somatosensory cortex, trunk region (S1Tr). Single-cell sequencing reveals that the S1Tr c-fos-positive neurons activated by acute stress are largely GABAergic somatostatin (Sst) neurons. These S1Tr^{Sst} neurons desensitize during subsequent anxiety-like behavior tests. Inhibiting or inducing apoptosis of S1Tr^{Sst} neurons mimics acute-stress effects and induces anxiety, while activating these neurons reduces acute-stress-induced anxiety. S1Tr^{Sst} cells receive inputs from secondary auditory cortex, dorsal area (AUD) GABAergic neurons to modulate this anxiety. Spatial transcriptome sequencing and targeted Pde4b protein knockdown show that acute stress reduces Pde4b-regulated cAMP signaling in AUD^{GABA}-S1Tr^{Sst} projections, leading to decreased S1Tr^{Sst} neuron activity in subsequent behavioral tests. Our study reports a neural and molecular mechanism for acute-stress-induced anxiety, providing a basis for treating anxiety disorders.

INTRODUCTION

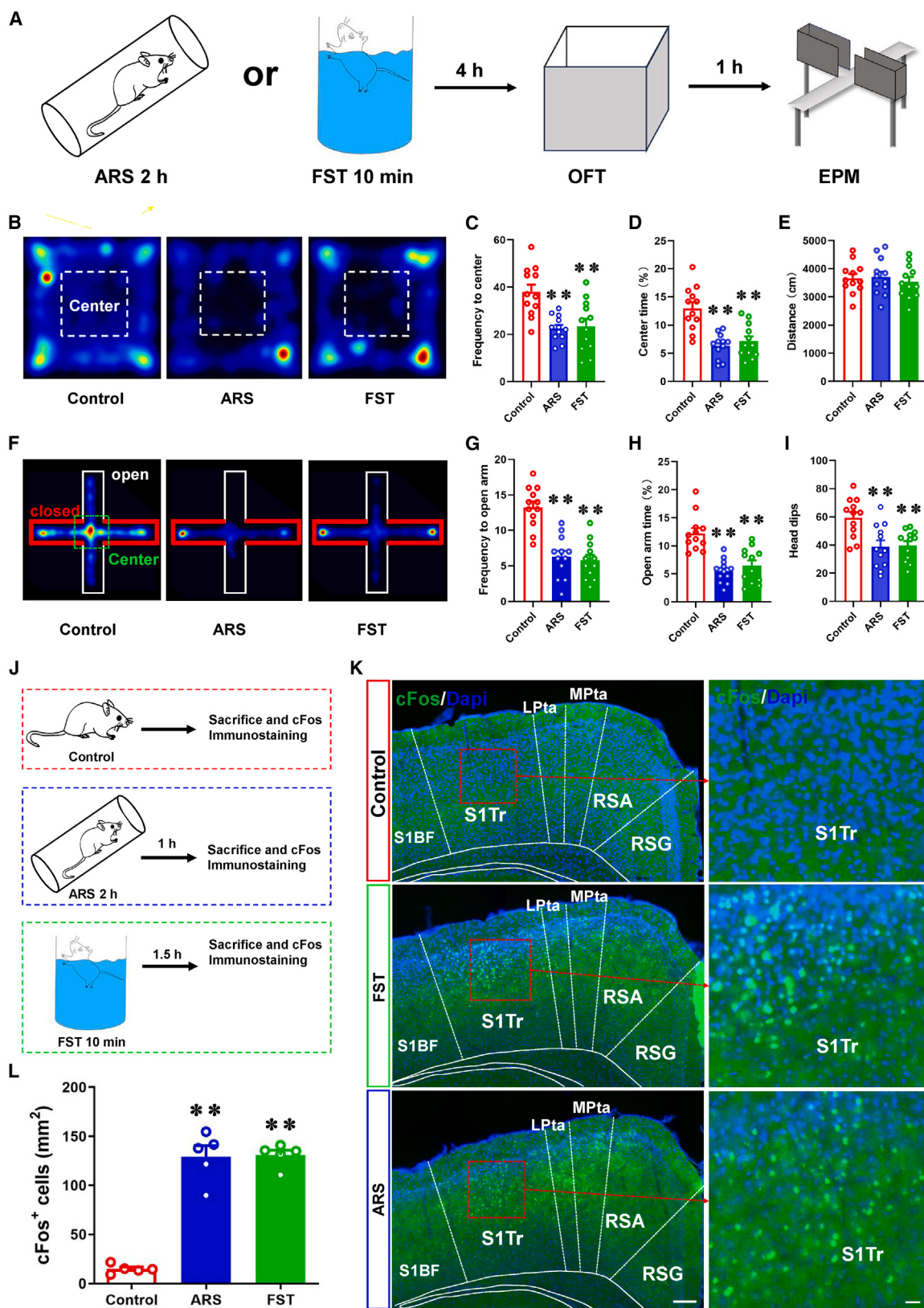
Anxiety is a complex emotion that manifests as excessive tension, worry, or fear in the face of uncertainty. It is an important warning mechanism for animals to avoid danger based on past group or individual survival experiences.¹ Typically, when mammals encounter acute-stress stimuli, they will produce temporary anxiety emotion to maintain the vigilance and arousal required to sustain attention, cope with emerging threats and challenges, and avoid repeated exposures to hazardous situations. Using acute-stress models and behavioral tests that exploit the “approach-avoidance” conflict, typically the open-field test (OFT) and the elevated plus maze (EPM),^{2–4} studies have identified many brain areas such as ventromedial prefrontal cortex, basolateral amygdala, and ventral hippocampus that work in concert to regulate anxiety-like behaviors.^{5–11} However, while previous studies have focused on the neural circuits linking stress to anxiety, the underlying mechanisms of why acute stress can regulate the neural circuits and thus cause anxiety are still insufficiently investigated.

The primary somatosensory cortex (S1) is the somatosensory center of the brain, which plays a key role in the processing of pain and anxiety-like behaviors.^{12–15} Studies have indicated

that inhibition of the S1 glutamatergic neurons that innervate caudal dorsolateral striatum (cDLS) GABAergic neurons alleviated chronic-pain-induced anxiety-like behavior¹²; activation of the parafascicular thalamic nucleus (Pf) neurons innervated by the S1 neurons could induce hyperalgesia and anxiety,¹³ suggesting that the S1 neurons play an important role in the modulation of anxiety. However, to date, it remains unclear whether S1 neurons are able to participate in acute-stress-induced anxiety.

In this study, we found that the somatostatin-positive cells of the S1 trunk region (S1Tr^{Sst}) were activated in large numbers by employing single-cell sequencing. We examined whether, how, and why the S1Tr^{Sst} neurons participate in the modulation of acute-stress-induced anxiety-like behavior by using calcium imaging, neuropharmacological, electrophysiological, spatial transcriptome sequencing, conditional mouse mutagenetic, opto-/chemogenetic, and precise projection- and synapse-specificity Pde4b protein knockdown strategies. Intriguingly, we demonstrated that acute stress increased the expression of Pde4b protein in S1Tr^{Sst} neuron inputs from AUD^{GABA} neurons, which leads to excessive degradation of cyclic adenosine monophosphate (cAMP), resulting in hypoactivity of S1Tr^{Sst} neurons during subsequent behavioral tests, thus producing anxiety.





(legend on next page)

RESULTS

Acute stress produces anxiety-like behavior and activates S1Tr neurons

To induce anxiety-like behavior in C57BL/6J mice, we performed the classic acute restraint stress (ARS) and forced swimming test (FST),^{16–18} after which we employed an OFT and EPM to assess the anxiety-like phenotype (Figure 1A). Results showed that in the OFT, the frequency to center and the time spent in center of the mice exposed to ARS or FST stress were significantly decreased compared with the control mice (Figures 1B–1D). Notably, we did not detect significant changes in locomotor activity among groups of mice with or without ARS or FST stress (Figure 1E). In the EPM test, mice subjected to ARS or FST stress exhibited significantly less frequency to open arm, time spent in open arm, and head dips than control mice (Figures 1F–1I). These results suggested that both ARS and FST stress produced significant anxiety-like effects in mice. Interestingly, using immunofluorescence staining, we found that a large number of neurons expressed c-fos protein in the S1Tr region after ARS or FST stress (Figures 1J–1L), suggesting that the neurons of S1Tr may be associated with acute-stress-induced anxiety.

The S1Tr c-fos-positive neurons activated by acute stress are largely Sst neurons

To examine whether the c-fos-positive neurons activated by acute stress in S1Tr were related to acute-stress-induced anxiety, we first wanted to clarify the types of these c-fos-positive neurons. To this end, we employed single-cell sequencing to analyze the marker genes expressed in S1Tr c-fos-positive neurons after acute stress. From a total of 21,186 nuclei in the 15 mice exposed to FST stress (Figures S1A–S1E), we divided 578 c-fos-positive neurons into three clusters: glutamatergic neurons, GABAergic neurons, and other neurons (Figures S2A and S2B). Surprisingly, GABAergic neurons accounted for the highest proportion of all c-fos-positive neurons, reaching 48.1% (Figures S2C–S2F), suggesting that the S1Tr GABAergic neurons may play an important role in stress-induced anxiety. Given GABAergic neurons are usually classified into three categories—vasoactive intestinal polypeptide (VIP) neurons, parvalbumin (Pvalb) neurons, and Sst neurons—we subsequently divided the c-fos-positive GABAergic neurons into four clusters based on the marker genes of the three categories (Figure S2G). Our results indicated that the Sst neurons were the most numerous, accounting for 53.9% of all c-fos-positive GABAergic neurons (Figures S2H–S2J). Together, these

data indicated that the S1Tr^{Sst} GABA cells were likely linked to the effects of acute stress.

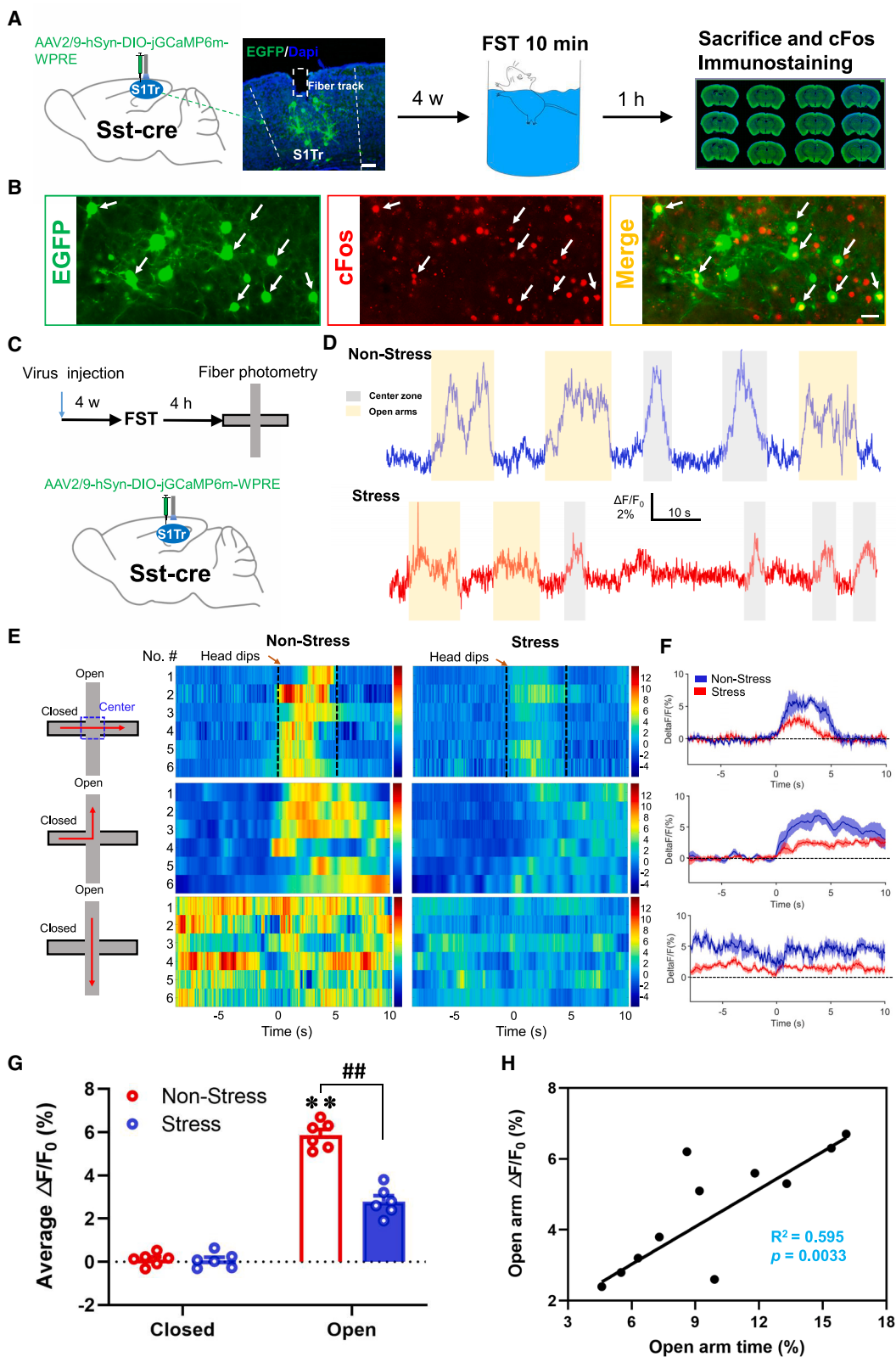
Acute-stress-induced anxiety correlates with the hypoactivity of S1Tr^{Sst} neurons

The results described above revealed that the S1Tr^{Sst} GABAergic neurons were massively activated by acute stress, so it is plausible to hypothesize that S1Tr^{Sst} GABAergic neurons could correlate with acute-stress-induced anxiety. To directly test this hypothesis, we utilized calcium imaging *in vivo* to assess whether acute stress would affect the real-time activity of S1Tr^{Sst} cells during anxiety-like behavior tests. We employed Sst-Cre mice carrying cyclization recombination enzyme (Cre) in Sst-expressing neurons as used in a previous study¹⁹ and utilized adeno-associated viruses (AAVs) carrying a DIO element that is dependent on Cre protein for the specific labeling and regulation of Sst-positive neurons. Calcium signal of the S1Tr^{Sst} neurons was recorded via photometry fibers implanted above the S1Tr of freely moving mice after injection of AAVs encoding Cre-inducible GCaMP6m into the S1Tr of Sst-Cre mice (Figure 2A). Four weeks later, the mice were subjected to FST stress followed by c-fos immunofluorescence staining 1 h later. The results showed that Sst neurons expressing green fluorescence had considerable colocalization with c-fos protein (Figure 2B), which further validated the results of single-cell sequencing analysis.

Subsequently, real-time calcium activity of control mice (“non-stress”) or mice exposed to FST stress (“stress”) were recorded during free movement of the closed arm, the central region, and the open arm in the EPM test (Figure 2C). Our results showed that when entering the central area and the open-arm area for exploratory behavior (especially the head-dip behavior), mice in both the non-stress group and the stress group exhibited remarkable calcium transients of the S1Tr^{Sst} neurons (Figures 2D–2G), which suggested that the S1Tr^{Sst} neurons were involved in anxiety-like behavior. However, compared with mice in the non-stress group, mice subjected to FST stress showed a reduced hyperactivity of the S1Tr^{Sst} neurons, correlating with the decreased duration in the open arm (Figures 2D–2H), suggesting that acute stress could induce desensitization of the S1Tr^{Sst} neurons. Statistical analyses indicated that the probability of S1Tr^{Sst} neuronal hyperexcitability was highly correlated with the duration of individual entry into the open arm (Figure 2H). Collectively, these results demonstrated that acute-stress-induced S1Tr^{Sst} neuronal hypoactivity was associated with the anxiety responses.

Figure 1. Acute physical stress generates anxiety-like behavior and activates S1Tr neurons

- (A) Experimental schedule for ARS or FST stress, followed 4 h later by OFT and another hour later by EPM.
 - (B) Heatmap representation of the time spent in OFT.
 - (C–E) The entries into the center zone (C), time spent in the center zone (D), and total distance traveled (E) in OFT.
 - (F) Heatmap representation of the time spent in EPM.
 - (G–I) The entries into the open arm (G), time spent in the open arm (H), and head-dip times (I) in EPM.
 - (J–L) Experimental schedule (J) and representative images (K) as well as graphs (L) of c-fos-positive neurons following FST and ARS stress. S1BF, primary somatosensory cortex, barrel field; LPta, lateral parietal association cortex; MPta, medial parietal association cortex; RSA, retrosplenial agranular cortex; RSG, retrosplenial granular cortex. Scale bar (left), 20 μm; scale bar (right), 200 μm.
- All values are presented as the mean ± SEM. ** $p < 0.01$ vs. control, Bonferroni post hoc test after one-way ANOVA (C: $F_{(2,33)} = 10.14, p = 0.0005$; D: $F_{(2,33)} = 16.54, p < 0.0001$; E: $F_{(2,33)} = 0.2559, p = 0.7758$; G: $F_{(2,33)} = 25.91, p < 0.0001$; H: $F_{(2,33)} = 14.33, p < 0.0001$; I: $F_{(2,33)} = 8.768, p = 0.0009$; L: $F_{(2,12)} = 85.02, p < 0.0001$).



(legend on next page)

Inhibition of S1Tr^{Sst} neurons mimics acute-stress effects to induce anxiety

Because acute-stress-induced anxiety-like behavior likely results from acute-stress-elicited desensitization in the S1Tr^{Sst} neurons as we have shown above, it is possible that inhibition of S1Tr^{Sst} neurons would mimic acute-stress-elicited anxiety. To test this hypothesis, we first employed an optogenetic strategy to inhibit S1Tr^{Sst} neurons in Sst-Cre mice. Before performing behavioral tests, electrophysiological methods were employed to determine whether optostimulation can effectively inhibit eNpHR3.0-expressing neurons. Sst-Cre mice receiving AAV2/9-DIO-eNpHR3.0-mCherry injection in the S1Tr were sacrificed for patch-clamp experiments on brain slices. Mice with virus injection showed confined mCherry-labeled Sst neurons in the S1Tr (Figures 3A and 3B). Results showed a significant reduction in the firing rates after yellow laser light stimulation (Figure 3C), suggesting not only a specific expression of eNpHR3.0 in the S1Tr^{Sst} neurons but also their inhibition by photostimulation.

Next, the effect of optoinhibition on anxiety in S1Tr^{Sst} neurons was investigated by injecting a virus into S1Tr and subsequently implanting a fiber photometer at an angle of 30° above it. When exposed to yellow laser light, mice showed significantly reduced frequency to the center and duration time in the center without significant changes in locomotor activity during the OFT (Figures 3D–3G). During the EPM test, mice with inhibition of S1Tr^{Sst} neurons exhibited significantly less frequency to open arms, time spent in open arms, and head dips than control mice (Figures 3H–3K). These results suggested that optoinhibition of S1Tr^{Sst} neurons produced significant anxiety-like effects in mice.

Subsequently, we investigated the effect of S1Tr^{Sst} neurons on anxiety by chemoinhibition. Sst-Cre mice were injected with AAV2/9-DIO-hM4Di-mCherry (AAV2/9-DIO-mCherry as control) into bilateral S1Tr, and the accurate expression of mCherry-positive neurons in S1Tr regions was confirmed (Figures 3L and 3M). Our data revealed that mice with chemoinhibition of S1Tr^{Sst} neurons exhibited significant anxiety-like effects in both OFT (Figures 3N–3P) and EPM (Figures 3R–3U) without significant changes in locomotor activity relative to control mice (Figure 3Q). Moreover, to further confirm the role of S1Tr^{Sst} neurons in anxiety, we examined whether S1Tr^{Sst} neuronal apoptosis could induce anxiety-like behaviors in mice. Sst-Cre mice received AAV2/9-hSyn-DIO-Caspase3-EGFP injection into bilateral S1Tr, which was followed 4 weeks later by behavioral tests (Figure S3A). The RNAscope results reveal that no EGFP- or Sst-positive neurons were detected in the S1Tr of the Caspase3

virus-injected group when compared to the control group, suggesting that Sst neurons in S1Tr were successfully ablated (Figure S3B). Consistent with our hypothesis, apoptosis of S1Tr^{Sst} neurons in mice produced significant anxiety-like behaviors in both OFT (Figures S3C–S3E) and EPM (Figures S3G–S3J) without significant changes in locomotor activity (Figure S3F). Together, these results revealed that inhibition of S1Tr^{Sst} neurons could mimic acute-stress effects to induce anxiety.

Activation of S1Tr^{Sst} neurons rescues both acute and chronic stress-elicited anxiety

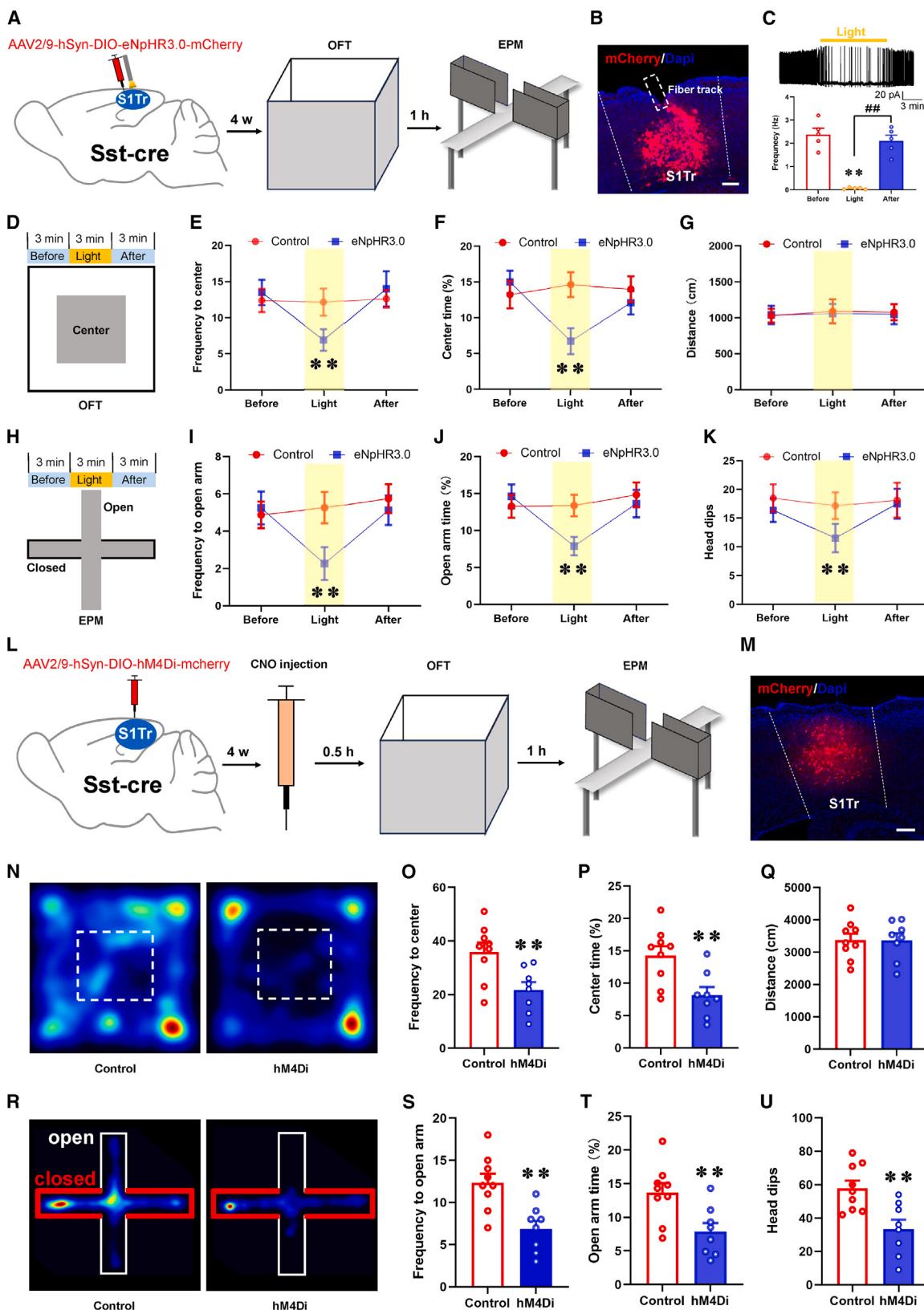
While inhibition of S1Tr^{Sst} neurons mimics stress effects to induce anxiety-like behavior, it is plausible to hypothesize that activation of S1Tr^{Sst} neurons would rescue stress-elicited anxiety-like behavior. To directly test this hypothesis, we decided to use both chemoactivation and optoactivation methods to activate S1Tr^{Sst} neurons. AAV2/9-DIO-hM3Dq-mCherry (Figure 4A) or AAV2/9-DIO-ChR2-EGFP (Figures 4K and S4A) were injected into bilateral S1Tr, followed by chemoactivation or optoactivation, respectively. We observed confined mCherry-labeled (Figure 4B) or GFP-labeled (Figures 4L and S4B) S1Tr neurons in mice with virus injection, suggesting that the brain areas where viruses were injected were accurate. Our results showed that neither chemoactivation (Figures 4C–4J) nor optoactivation (Figures S4C–S4H) of S1Tr^{Sst} neurons could induce any behavioral changes in OFT and EPM tests in mice of the non-stress group, which suggested that activation of S1Tr^{Sst} neurons did not produce significant effects on anxiety-like behavior in normal mice. However, when S1Tr^{Sst} neurons were activated by CNO injection (Figures 4C–4J) or blue laser irradiation (Figures 4M–4T), mice in the stress group exhibited significant anti-anxiety effects against acute stress in both OFT and EPM without significant effects on locomotor activity, suggesting that activation of S1Tr^{Sst} neurons could rescue acute stress-elicited anxiety-like behavior. Moreover, similar to acute stress, the chemoactivation of S1Tr^{Sst} neurons was capable of ameliorating anxiety-like behaviors induced by chronic physical stress (Figures S5A–S5H). These results indicate that S1Tr^{Sst} neurons are involved in regulating both acute and chronic stress-induced anxiety-like behavior.

S1Tr^{Sst} neurons receive direct inputs from AUD to modulate acute-stress-induced anxiety

After confirming the sufficient and necessary functions of S1Tr^{Sst} neurons in acute-stress-elicited anxiety, we further verified the upstream circuit of S1Tr^{Sst} neurons. We first tracked and imaged

Figure 2. Acute-stress-induced anxiety correlates with the desensitization of the S1Tr^{Sst} neurons

- (A) Experimental schedule for viral injections into unilateral S1Tr with optical fiber implantation, followed 4 weeks later by FST stress and 1 h later by sacrifice and immunostaining in Sst-cre mice. Frontal sections show EGFP-labeled Sst neurons in the BLA. Scale bar, 100 μm.
 - (B) EDIFP-labeled S1Tr^{Sst} neurons (green) colocalized with c-fos protein (red) expression in Sst-cre mice exposed to acute stress. Scale bar, 20 μm.
 - (C) Experimental scheme of virus injection and fiber photometry tests.
 - (D) Examples of *in vivo* fluorescence changes of S1Tr^{Sst} neurons during EPM behavior test.
 - (E) Example behavioral trajectories between arm compartments (left) and heatmaps of S1Tr^{Sst} normalized Ca²⁺ activity during those trajectories (right). Arrows indicate a head-dip behavioral event in the center.
 - (F) Dynamics of GCamp6 signal 8 s before and 10 s after the mice enter EPM center and open arms.
 - (G) Statistics of the average Ca²⁺ fluorescence signaling changes in the closed and open arms of the EPM between mice in stress group and non-stress group.
 - (H) Correlation between the strength of S1Tr^{Sst} neurons' calcium transients and the duration of the stressed mice in the open arm of EPM.
- All values are presented as the mean ± SEM. ***p* < 0.01 vs. non-stress group; #*p* < 0.01, Bonferroni post hoc test after two-way ANOVA (G: arm: *F*_(1,20) = 418.1, *p* < 0.0001; si-Pde4b: *F*_(1,20) = 56.80, *p* < 0.0001; interaction: *F*_(1,20) = 53.81, *p* < 0.0001).



(legend on next page)

the whole brain with high-throughput techniques using AAV-Retro (Figure S6A) and found that S1Tr receives a large amount of input from the secondary auditory cortex, dorsal area (AUD), secondary motor cortex (M2), and claustrum (CL), and a small amount from the entorhinal cortex (ECT), ventral orbital cortex (VO), medial orbital cortex (MO), lateral orbital cortex (LO), and medial orbital cortex (PrL) (Figures S6B and S6C). To determine which of the aforementioned brain regions can directly innervate S1Tr^{Sst} neurons, we injected Cre-dependent helper viruses (AAV2/9-DIO-EGFP-TVA and AAV2/9-DIO-RVG, which enables retrograde transport of the rabies virus across the monosynapse) into the S1Tr of Sst-Cre mice,^{20,21} followed 3 weeks later by an injection of rabies virus (RV-Enva-ΔG-mCherry) at the same site, and another 1 week later by sacrifice of the mice and subsequent high-throughput whole-brain imaging (Figure 5A). We identified starter cells (GFP⁺mCherry⁺) in the S1Tr (Figure 5B, white arrowheads) and mapped the presynaptic cells (mCherry⁺) in the AUD, VO, and M2, which suggested that S1Tr^{Sst} neurons receive monosynaptic inputs from AUD, VO, and M2 (Figure 5C).

To identify presynaptic partners of S1Tr^{Sst} inputs that modulate acute-stress-elicited anxiety, we employed Sst-Cre mice and a trans-synaptic tagging strategy²² for a specific transgene expression in S1Tr^{Sst} neurons input from AUD, VO, and M2, respectively. Mice were injected with AAV2/1-hSyn-DIO-Flp-EGFP into bilateral AUD, VO, or M2, followed by AAV2/9-EF1a-fDIO-eNpHR3.0-mCherry (or AAV2/9-EF1a-fDIO-mCherry as control) injection into bilateral S1Tr (Figures 5D, S8A, and S8I). This strategy gave rise to eNpHR3.0-mCherry expression in S1Tr^{Sst} neurons innervated by AUD, VO, or M2, and the specificity of this intersectional strategy was verified in control experiments (Figures S7A–S7D). We observed confined mCherry-labeled S1Tr neurons and GFP-labeled AUD, VO, and M2 neurons in mice with virus injection (Figures 5E, S8B, and S8J), which suggested that the brain areas where viruses were injected were accurate. We then assessed OFT and EPM testing behaviors. Surprisingly, in response to yellow laser stimulation, only mice with optoinhibited AUD-S1Tr^{Sst} synapses displayed significant anxiety-like behavior in both OFT and EPM without significant effects on locomotor activity (Figures 5F–5M). Neither mice with optoinhibited S1Tr^{Sst} neurons innervated by VO (Figures S8C–S8H) nor innervated by M2 (Figures S8K–S8P) exhibited any anxiety-like behavior in OFT and EPM. Taken together, these results indicated that S1Tr^{Sst} neurons receive direct inputs from AUD to modulate acute-stress-induced anxiety.

Figure 3. S1Tr^{Sst} neuron inhibition induced anxiety-like behavior

(A and L) Experimental schedule for photoinhibition (A) and chemoinhibition (L) virus injection and subsequent behavioral tests.

(B and M) Frontal sections show mCherry-labeled cells in the S1Tr. Scale bars, 100 μm.

(C) Decreased excitability of eNpHR3.0-expressing cells by yellow light.

(D) Schematic diagram of the OFT for photoinhibition.

(E–G) The entries into the center zone (E), time spent in the center zone (F), and total distance traveled (G) in OFT.

(H) Schematic diagram of the EPM test for photoinhibition.

(I–K) The entries into the open arm (I), time spent in the open arm (J), and head-dip times (K) in EPM.

(N) Heatmap representation of the time spent in OFT.

(O–Q) The entries into the center zone (O), time spent in the center zone (P), and total distance traveled (Q) in OFT.

(R) Heatmap representation of the time spent in EPM.

(S–U) The entries into the open arm (S), time spent in the open arm (T), and head-dip times (U) in EPM.

All values are presented as the mean ± SEM. Bonferroni post hoc test after one-way ANOVA (C: ***p* < 0.01 vs. before, ##*p* < 0.01; *F*_(2,12) = 35.85, *p* < 0.0001. E–G, I–K: ***p* < 0.01 vs. control + light group, two tailed t test. O–Q, S–U: ***p* < 0.01 vs. control group, two tailed t test).

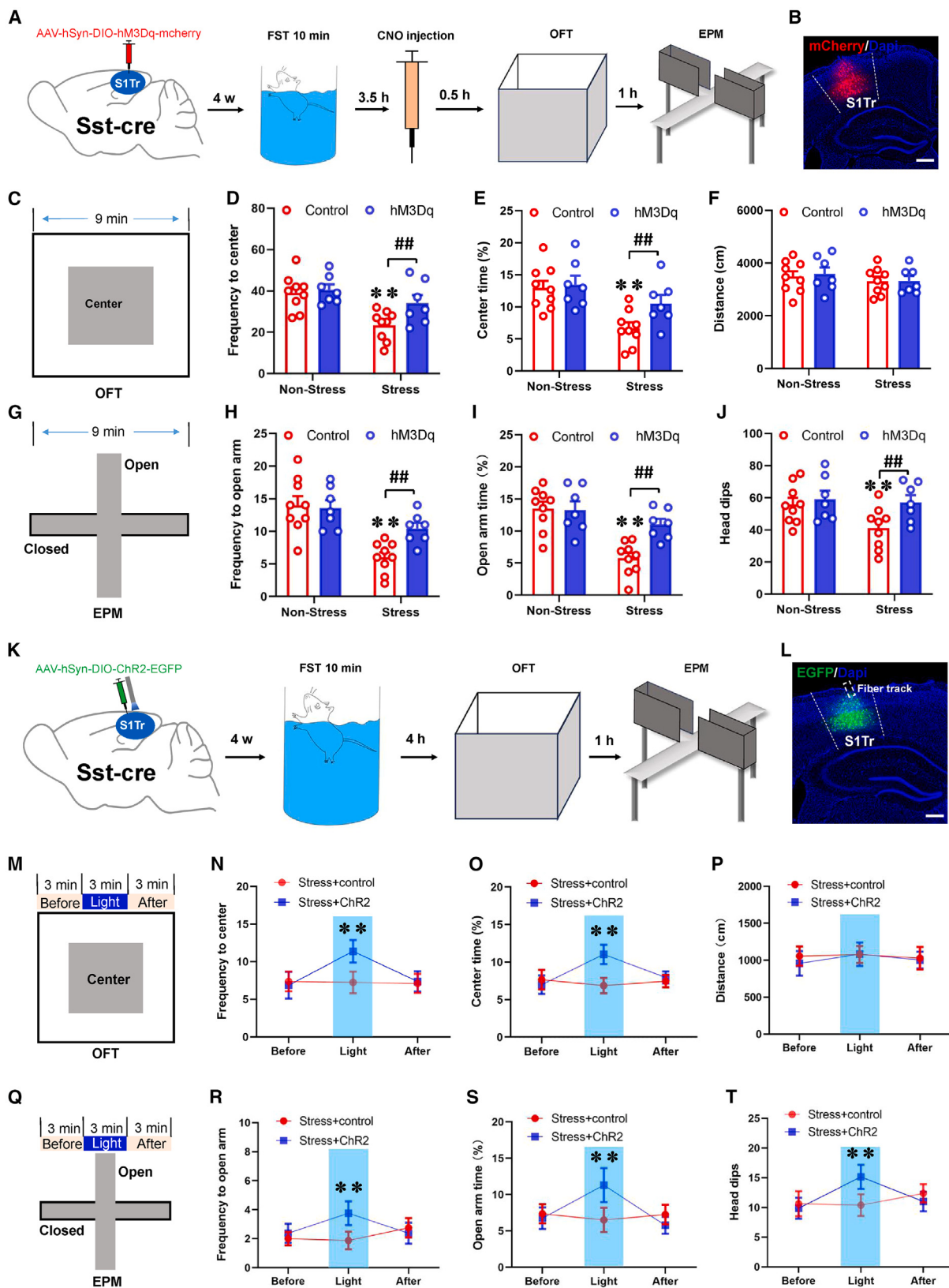
AUD^{GABA} neurons that innervate S1Tr^{Sst} neurons participate in acute-stress-induced anxiety

The aforementioned data indicated that S1Tr^{Sst} neurons involved in the regulation of acute-stress-induced anxiety received projections from AUD neurons. Next, we intended to identify the types of AUD neurons that directly innervate S1Tr^{Sst} neurons. To this end, we injected helper viruses (AAV2/9-DIO-EGFP-TVA and AAV2/9-DIO-RVG) into unilateral S1Tr, followed 3 weeks later by an injection of rabies virus (RV-Enva-ΔG-mCherry) at the same location and another 1 week later by RNAscope and confocal microscopy imaging (Figure 6A). Solute carrier family 17, member 1 (Slc17a7, which encodes vesicular glutamate transporter 1) was utilized as a marker gene of glutamatergic neurons and solute carrier family 32, member 1 (Slc32a1, which encodes vesicular GABA transporter, VGAT) was utilized as a marker of GABAergic neurons. Surprisingly, our results demonstrated that AUD mCherry-positive neurons have an obvious colocalization with Slc32a1 but not with Slc17a7 (Figure 6B), suggesting that the AUD neurons innervating S1Tr^{Sst} were GABAergic inhibitory neurons.

Subsequently, we examined whether inhibition of S1Tr-projecting AUD^{GABA} neurons could remove the inhibition of AUD on S1Tr^{Sst} neurons and thus prevent anxiety-like behaviors induced by acute stress. We injected AAV2/Retro-hSyn-Cre-mCherry into bilateral S1Tr, followed by an injection of AAV2/9-VGAT-DIO-hM4Di-EGFP into bilateral AUD and another 4 weeks later by OFT and EPM testing (Figure 6C). Confined mCherry-labeled S1Tr neurons and GFP-labeled AUD^{GABA} neurons were observed in mice with virus injection, indicating that the brain areas where viruses were injected were accurate (Figure 6D). As expected, chemoinhibiting AUD^{GABA} neurons had no effect on the behavioral performance of non-stressed mice in OFT and EPM (Figures 6E–6J). However, in mice receiving acute stress, chemoinhibiting AUD^{GABA} neurons alleviated the anxiety-like behavior in both OFT (Figures 6E and 6F) and EPM (Figures 6H–6J) without significant effects on locomotor activity (Figure 6G). These results together indicate that AUD^{GABA} neurons innervating S1Tr^{Sst} neurons participate in acute-stress-induced anxiety.

Acute stress causes downregulation of PDE-mediated cAMP signaling pathways in the S1Tr^{Sst} neurons innervated by AUD^{GABA}

The data reported above revealed that acute stress could cause desensitization of S1Tr^{Sst} neurons innervated by AUD^{GABA},



(legend on next page)

which makes these S1Tr^{Sst} neurons hypoactive during the anxiety behavioral test, resulting in anxiety-like behavior in mice. However, we still did not know why acute stress could provoke hypoactivity in the S1Tr^{Sst} neurons innervated by AUD^{GABA} during the anxiety behavioral test. To solve this problem, we initially injected AAV2/1-DIO-FLP virus into AUD and AAV2/9-EF1a-fDIO-eNpHR3.0-mCherry virus into the bilateral S1Tr to specifically label S1Tr^{Sst} neurons innervated by AUD^{GABA}, followed by FST stress and spatial transcriptome sequencing (Figure S10A). After obtaining and analyzing the genes expressed in all spots, we then identified the spots in the S1Tr of both non-stressed and stressed groups that contained specific viral element sequences and subsequently analyzed the differentially expressed genes between them (Figures S9A–S9F and S10B). The volcano plot results revealed that the expression of a substantial number of genes in S1Tr^{Sst} neurons innervated by AUD^{GABA} of mice underwent significant changes 2 h after FST stress (Figure S10C). Subsequently, we performed Kyoto Encyclopedia of Genes and Genomes (KEGG) and gene ontology (GO) enrichment analysis to cluster these differentially expressed genes (Figures S10D–S10G). Remarkably, there were noteworthy alterations observed in the cAMP signaling pathway among these differential genes, particularly involving multiple phosphodiesterase (PDE) proteins (which can hydrolyze cAMP in the cytoplasm and reduce the biochemical action conducted by cAMP²³) such as Pde4b, Pde1a, and Pde10a within this signaling pathway. Notably, both Pde4b and Pde10a exhibited a significant increase in expression levels within the stressed group of mice (Figures S10H–S10J), and we verified through an ELISA experiment that the cAMP content in the S1Tr of acutely stressed mice was significantly reduced (Figure S10K), suggesting that acute stress could reduce the functions of the cAMP signaling pathway by enhancing PDE protein expression.

Knockout of Pde4b in AUD^{GABA}-S1Tr^{Sst} neural circuit reduces acute-stress-elicited anxiety and neuronal hypoactivity

As a second messenger that responds to external stimuli, the cAMP signaling pathway is closely related to neuronal calcium activity, neurotransmitter synthesis and release, and other functions.^{24–27} The regulation of intracellular cAMP concentration is

mainly determined by the balance between the hydrolysis of cyclic nucleotide PDEs and the synthesis of adenylate cyclase.²³ If this balance is broken, cells cannot accurately respond to external stimuli. As our results thus far demonstrate that acute stress increases the expression of Pde4b and Pde10a in S1Tr^{Sst} neurons innervated by AUD^{GABA}, it is possible that the increased expression of these PDEs leads to excessive hydrolysis of cAMP, resulting in weakened function of the cAMP signaling pathway, ultimately causing neuronal desensitization and anxiety-like behavior. Considering the more significant increase in Pde4b expression than Pde10a in S1Tr^{Sst} neurons innervated by AUD^{GABA} after acute stress, we designed a projection- and cell-type-specific Pde4b-microRNA knockdown (si-Pde4b) AAV to knock out Pde4b in S1Tr^{Sst} neurons. After verifying that these AAVs were indeed effective in reducing Pde4b expression in cultured cortical neurons (Figures S11A–S11E), we injected AAV2/1-hSyn-Flp-mCherry into bilateral AUD, followed by an injection of AAV2/9-fDIO-miR-155(Pde4b)-EGFP (or AAV2/9-fDIO-EGFP as control) into bilateral S1Tr and subsequent OFT and EPM behavioral tests (Figure 7A). Mice with virus injection showed confined mCherry-labeled AUD neurons and EGFP-labeled S1Tr neurons (Figure 7B). Levels of Pde4b expression in neurons infected with the control virus did not significantly differ from those in neighboring uninfected neurons (Figure 7C). However, levels of Pde4b expression in neurons infected with si-Pde4b viruses were significantly lower than those in neighboring uninfected neurons (Figures 7D and 7E), indicating an effective reduction of Pde4b expression in S1Tr^{Sst} neurons. Consistent with our hypothesis, knockout of Pde4b genes in AUD^{GABA}-S1Tr^{Sst} neural circuit produced significant resistant effects against acute-stress-induced anxiety-like behavior in both OFT (Figures 7F and 7G) and EPM (Figures 7I–7K) without significant effects on locomotor activity (Figure 7H).

To verify whether knockdown of Pde4b genes in AUD^{GABA}-S1Tr^{Sst} neural circuit can rescue the desensitization of S1Tr^{Sst} neurons during anxiety-like behavior testing in stressed mice, AAV2/1-hSyn-Flp-mCherry was injected into unilateral AUD, followed by an injection of AAV2/9-fDIO-miR-155(Pde4b)-EGFP and AAV2/9-fDIO-jGCaMP6m into unilateral S1Tr and then implanted optical fiber. Four weeks later, mice were subjected to

Figure 4. S1Tr^{Sst} neuron activation rescued acute-stress-induced anxiety-like behavior

(A and K) Experimental schedule for chemoactivation (A) and photoactivation (K) virus injection and subsequent behavioral tests.

(B and L) Frontal sections show mCherry-labeled cells (B) and EGFP-labeled neurons (L) in the S1Tr. Scale bars, 200 μm.

(C) Schematic diagram of the OFT for chemoactivation.

(D–F) The entries into the center zone (D), time spent in the center zone (E), and total distance traveled (F) in OFT.

(G) Schematic diagram of the EPM test for chemoactivation.

(H–J) The entries into the open arm (H), time spent in the open arm (I), and head-dip times (J) in EPM.

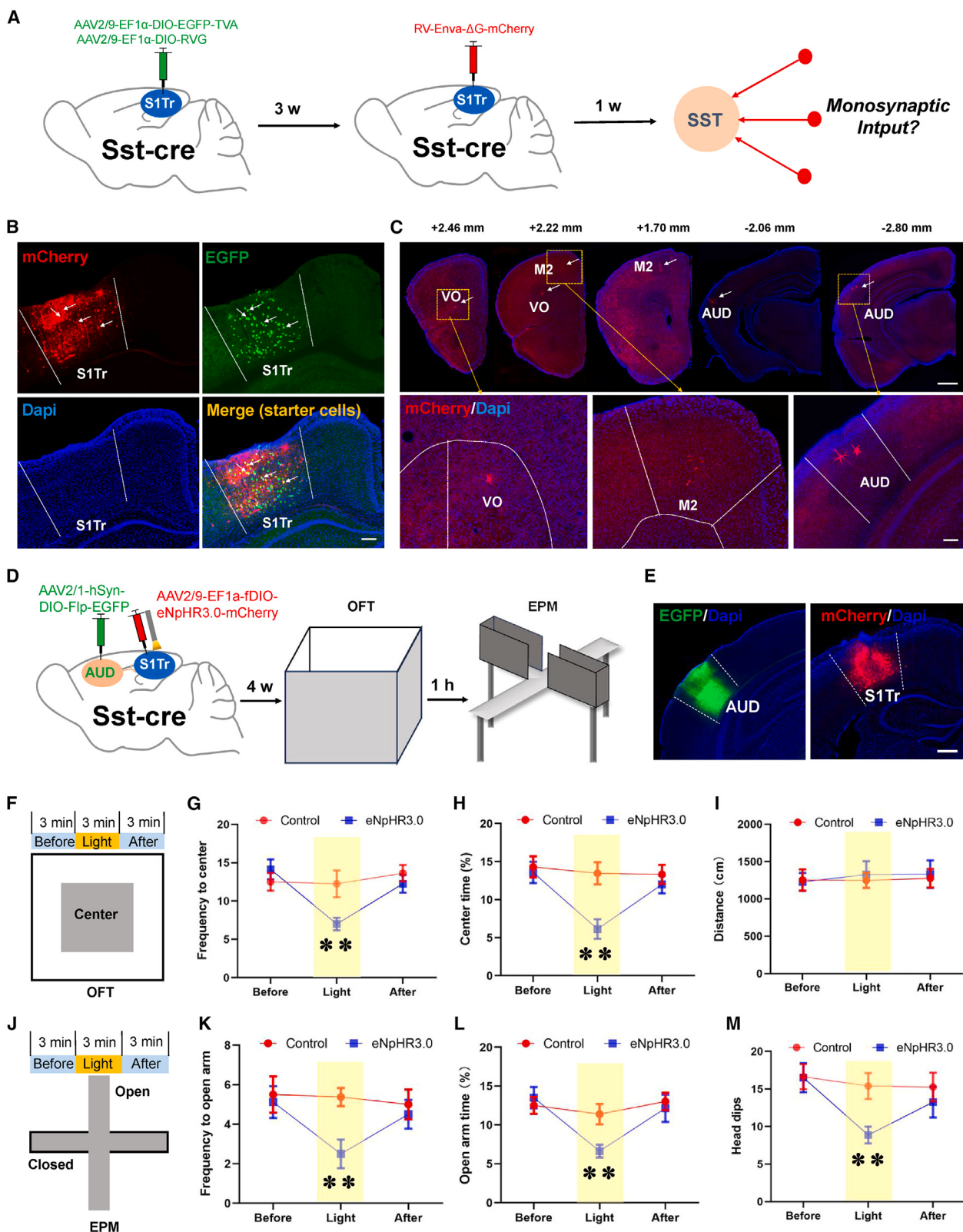
(M) Schematic diagram of the OFT for photoactivation.

(N–P) The entries into the center zone (N), time spent in the center zone (O), and total distance traveled (P) in OFT.

(Q) Schematic diagram of the EPM test for photoactivation.

(R–T) The entries into the open arm (R), time spent in the open arm (S), and head-dip times (T) in EPM.

All values are presented as the mean ± SEM. ** $p < 0.01$ vs. non-stress group, # $p < 0.01$; Bonferroni post hoc test after two-way ANOVA (D: stress: $F_{(1,28)} = 13.98$, $p = 0.0008$; hM3Dq: $F_{(1,28)} = 4.232$, $p = 0.0491$; interaction: $F_{(1,28)} = 2.443$, $p = 0.1293$. E: stress: $F_{(1,28)} = 15.36$, $p = 0.0005$; hM3Dq: $F_{(1,28)} = 3.550$, $p = 0.0699$; interaction: $F_{(1,28)} = 2.087$, $p = 0.1597$. F: stress: $F_{(1,28)} = 1.213$, $p = 0.2802$; hM3Dq: $F_{(1,28)} = 0.06693$, $p = 0.7977$; interaction: $F_{(1,28)} = 0.04309$, $p = 0.8370$. H: stress: $F_{(1,28)} = 24.67$, $p = 0.0391$; hM3Dq: $F_{(1,28)} = 3.179$, $p = 0.0854$; interaction: $F_{(1,28)} = 4.688$, $p = 0.0391$. I: stress: $F_{(1,28)} = 22.33$, $p < 0.0001$; hM3Dq: $F_{(1,28)} = 5.787$, $p = 0.0230$; interaction: $F_{(1,28)} = 6.677$, $p = 0.0153$. J: stress: $F_{(1,28)} = 3.380$, $p = 0.0766$; hM3Dq: $F_{(1,28)} = 4.474$, $p = 0.0434$; interaction: $F_{(1,28)} = 1.952$, $p = 0.1733$ and two tailed t test (G–I, K–M: ** $p < 0.01$ vs. control + light group).



(legend on next page)

FST stress, followed by EPM test and real-time calcium signal recording (Figure 7L). Interestingly, when entering the open-arm area for exploratory behavior, stressed mice with knockout of Pde4b genes in S1Tr^{Sst} neurons innervated by AUD^{GABA} exhibited significantly increased intensity of calcium transients compared with control stressed mice (Figures 7M–7O), which suggested that the augmentation of calcium signal transients was achieved by inhibiting the expression of Pde4b genes in the AUD^{GABA}-S1Tr^{Sst} neural circuit in stressed mice. Taken together, these results indicate that knockout of Pde4b in the AUD^{GABA}-S1Tr^{Sst} neural circuit reduces acute-stress-elicited anxiety and neuronal hypoactivity.

DISCUSSION

The presence of acute-stress stimuli can elicit transient anxiety in mammals, serving to sustain attention and effectively cope with emerging threats and challenges. However, the specific mechanisms that are responsible for acute-stress-induced anxiety are largely not clear. In this study, we observed a substantial activation of Sst neurons in the S1Tr region following exposure to acute stress. These S1Tr^{Sst} neurons, which were activated by acute stress, exhibited desensitization during subsequent anxiety-like behavior testing, characterized by a significant hypoactivity in the calcium transients. Meanwhile, we demonstrated that inhibition of S1Tr^{Sst} neurons could mimic the acute stress effect to induce anxiety-like behavior, whereas activation of S1Tr^{Sst} neurons could alleviate acute-stress-induced anxiety. Moreover, we indicated that these S1Tr^{Sst} neurons involved in acute-stress-induced anxiety receive innervation from GABAergic inhibitory neurons in the AUD. Finally, our results revealed an upregulation of several PDEs in the AUD^{GABA}-S1Tr^{Sst} neural circuit following acute stress exposure, resulting in a decreased activity of cAMP signaling pathway. Knockdown of Pde4b protein in the AUD^{GABA}-S1Tr^{Sst} neural circuit was able to reverse anxiety-like behavior and neuronal hypoactivity induced by acute stress. Together, these findings establish pivotal roles of S1Tr^{Sst} neurons in acute-stress-elicited anxiety and its underlying mechanisms.

The primary somatosensory cortex is situated in the posterior parietal lobe and is subdivided into several subregions, such as the hindlimb area, forelimb area, and trunk area. These subregions contain approximately 70% excitatory neurons and 30% inhibitory neurons and assume a central function in the management of sensory information from various parts of the body.^{28,29} Recently, a converging body of literature has suggested that the S1 also plays an important role in anxiety processing. Studies re-

vealed that activating the glutamatergic neurons in the hindlimb region of S1 (S1HL) projecting to cDLS exhibited anxiety-like behaviors,¹² while inhibition of S1HL glutamatergic neurons produced remission effects on chronic pain-induced anxiety disorder,¹³ demonstrating that glutamatergic neurons of the S1 are involved in stress-elicited anxiety. However, in our study, the results indicated that acute stress activates a large number of GABAergic Sst-positive neurons. Inhibition of the S1Tr^{Sst} neurons produced anxiety-like behaviors, while activating the S1Tr^{Sst} neurons could rescue the anxiety caused by acute and chronic stress, indicating that the inhibitory S1Tr^{Sst} neurons are involved in the regulation of anxiety-like behaviors induced by acute and chronic stress. Recent studies have revealed that both chronic restraint stress and acute sleep deprivation stress induce an upregulation of the excitatory receptor N-methyl-D-aspartate receptor (NMDAR) and a downregulation of the inhibitory receptor GABA type A receptor subunit $\alpha 1$ (GABAAR $\alpha 1$) in S1 neurons,³⁰ suggesting that acute or chronic physical stress is capable of disrupting the equilibrium of excitation and inhibition in S1. Incorporating our findings, it is likely that the decreased activity of S1Tr^{Sst} neurons during subsequent anxiety-like behavior tests might lead to the disinhibition of glutamatergic neurons, thereby causing their activation. It should be noted that activation of the S1Tr^{Sst} neurons did not generate a greater anti-anxiety effect in non-stressed mice, which may have resulted from a ceiling effect. Importantly, we also noticed that the S1Tr^{Sst} neurons activated by acute stress exhibited desensitization with a significant decrease in calcium transient intensity during the subsequent EPM test, which may explain why mice exposed to acute stress exhibited anxiety phenotypes in the subsequent behavior tests.

Our results reveal a striking short-range inhibitory neural circuit in the cerebral cortex involved in acute-stress-induced anxiety, as inhibition of AUD^{GABA}-S1Tr^{Sst} neurons but not M2-S1Tr^{Sst} or VO-S1Tr^{Sst} neurons generated avoidance behavior in anxiety tasks. The neural networks of different subregions of S1 projecting and projected are not entirely the same, which adds difficulty to studying the related functions of the neural circuits of S1. In view of this, we restricted the scope of our study to the trunk region of S1, a region that is significantly activated by acute stress. Surprisingly, our pseudotyped rabies-based tracing studies indicated that S1Tr^{Sst} neurons only receive monosynaptic inputs from three cortical nuclei: AUD, VO, and M2. Moreover, inhibiting S1Tr^{Sst} neurons innervated by AUD produced anxiety-like behavior, while inhibition of SST neurons innervated by M2 or VO did not result in behavioral changes. We inferred that Sst

Figure 5. S1Tr^{Sst} neurons receive direct inputs from AUD to regulate acute-stress-induced anxiety

- (A–C) Retrograde tracing of inputs to S1Tr^{Sst} neurons. (A) Viral injection strategy for labeling S1Tr^{Sst} neurons. (B) Sst-Cre mice were injected with helper virus followed by pseudotyped G-deleted rabies virus in the S1Tr. White arrowheads denote starter cells, which are positive for both GFP (helper) and mCherry (rabies). Representative images for three independent animals. Scale bar, 100 μ m. (C) Presynaptic partners were identified in the VO, M2, and AUD. Representative images for three independent animals. Scale bar, 200 μ m.
 - (D) Experimental schedule for virus injection and optical fiber implantation, followed 4 weeks later by OFT and 1 h later by EPM.
 - (E) Frontal sections show mCherry or EGFP labeling in S1Tr and AUD. Scale bar, 200 μ m.
 - (F) Schematic diagram of the OFT for photoinhibition.
 - (G–I) The entries into the center zone (G), time spent in the center zone (H), and total distance traveled (I) in OFT.
 - (J) Schematic diagram of the EPM test for photoinhibition.
 - (K–M) The entries into the open arm (K), time spent in the open arm (L), and head-dip times (M) in EPM.
- All values are presented as the mean \pm SEM (G–I, K–M; ** p < 0.01 vs. control + light group, two tailed t test).

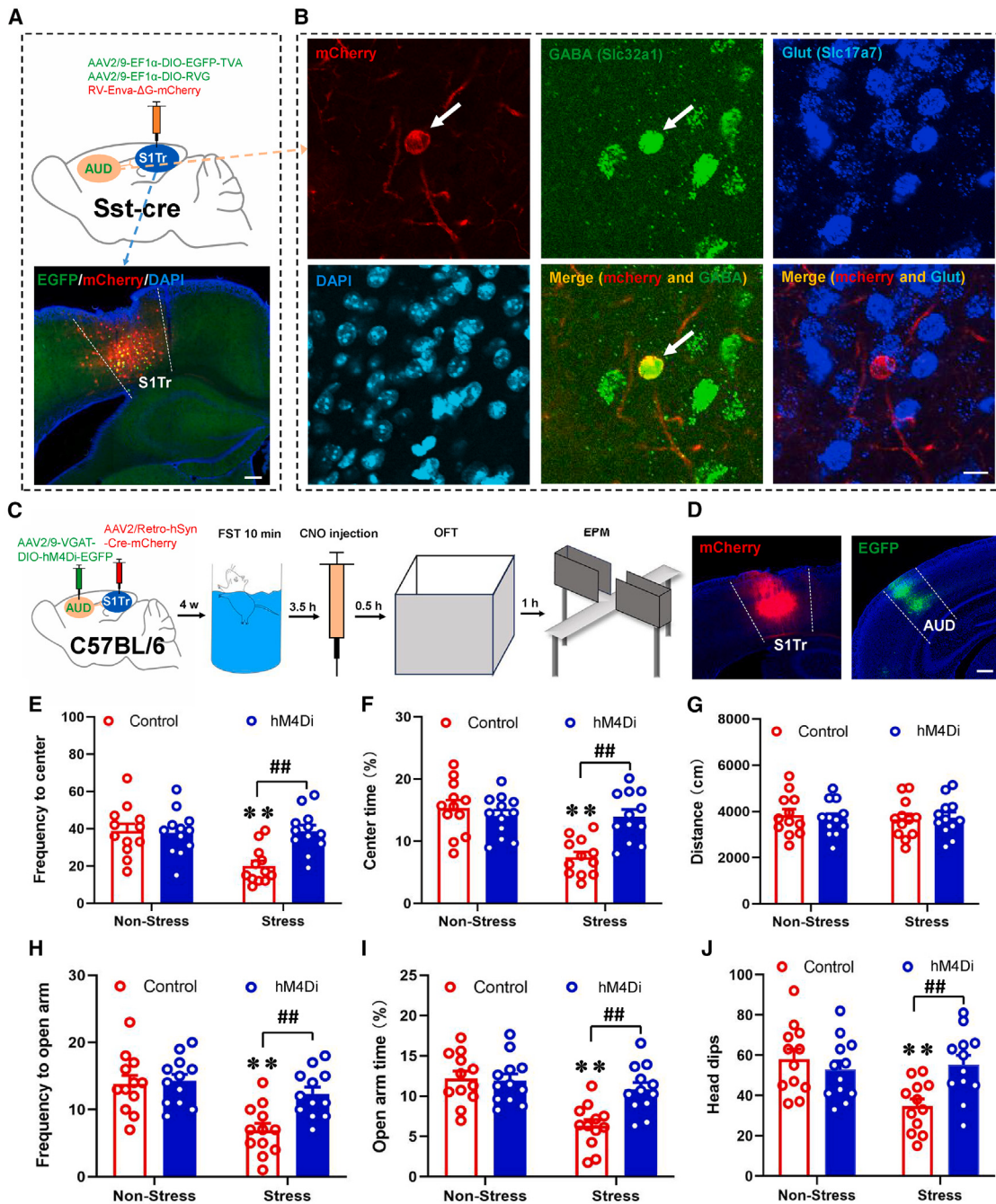


Figure 6. AUD^{GABA} neurons that inputs to S1Tr^{Sst} neurons participates in acute-stress-induced anxiety

(A) Top: schematic of sagittal sections showing viral injections into S1Tr. Bottom: frontal sections showing mCherry and EGFP labeling (starter cells) in S1Tr. Scale bar, 200 μ m.

(B) RNAscope results showed that mCherry neurons were colocalized with GABA but not glutamate in the AUD. White arrows indicate colabeled neurons. Scale bar, 20 μ m.

(C) Experimental schedule for chemoinhibition virus injection and subsequent behavioral tests.

(D) Frontal sections show mCherry-labeled cells in S1Tr and EGFP-labeled neurons in AUD. Scale bar, 200 μ m.

(E–G) The entries into the center zone (E), time spent in the center zone (F), and total distance traveled (G) in OFT.

(H–J) The entries into the open arm (H), time spent in the open arm (I), and head-dip times (J) in EPM.

All values are presented as the mean \pm SEM. ** p < 0.01 vs. non-stress group, ## p < 0.01; Bonferroni post hoc test after two-way ANOVA (E: stress: $F_{(1,44)} = 7.176$, $p = 0.0103$; hM4Di: $F_{(1,44)} = 7.044$, $p = 0.0110$; interaction: $F_{(1,44)} = 8.567$, $p = 0.0054$. F: stress: $F_{(1,44)} = 14.57$, $p = 0.0004$; hM4Di: $F_{(1,44)} = 6.211$, $p = 0.0165$; interaction: $F_{(1,44)} = 13.66$, $p = 0.0006$. G: stress: $F_{(1,44)} = 0.08735$, $p = 0.7690$; hM4Di: $F_{(1,44)} = 0.02617$, $p = 0.8722$; interaction: $F_{(1,44)} = 0.2073$, $p = 0.6512$.

(legend continued on next page)

neurons in S1Tr might exist in different functional clusters, and the S1Tr^{Sst} neuron clusters receiving AUD projections were likely not the same as those receiving M2 or VO, which could account for why S1Tr^{Sst} neuron inputs from AUD are the sole neuron cluster involved in acute-stress-induced anxiety.

For a long time, studies on the secondary auditory cortex (AU), including the dorsal area (AUD) and ventral area (AVU) in mice, have focused on its regulation of sound and auditory-related functions.^{31,32} So far, it has remained unclear whether AU had effects on emotional functions such as anxiety and depression. Our pseudotyped rabies-based tracing combined with RNA-scope results showed that GABAergic neurons in AUD but not AVU output to the S1Tr^{Sst} neurons, and inhibition of AUD^{GABA} neurons projecting to S1Tr, exhibited significantly resistant effects against acute-stress-induced anxiety. Our data indicate for the first time that the AUD region is involved in the regulation of anxiety in mouse, and its GABAergic neurons modulate anxiety emotions by inhibiting nearby downstream S1Tr^{Sst} neurons.

In this paper, we provide evidence indicating the important functions of intracellular PDEs modulating the cAMP signaling pathway in acute-stress adaptation and behavioral regulation. The cAMP signaling pathway is an important integrator of actions from various neurotransmitters, critically regulating functions including stress, depression, and cognition.^{24,33,34} Extracellular neurotransmitters stimulate the receptors, which in turn trigger cAMP synthesis through adenylyl cyclases.³⁵ cAMP hydrolysis by PDEs would counteract the function of adenylyl cyclase, thereby reducing cAMP levels. The activity of the cAMP/protein kinase A (PKA) cascade is tightly controlled to maintain the specificity and integrity of the intracellular signal propagation.³⁶ Our study complements previous evidence indicating that enhancement of the PDE-controlled cAMP signaling activity improves brain functions and stress-induced behavioral modulation. Moreover, unlike previous studies that focused on all neurons in a given brain region, we used AAVs with precise projection and synapse specificity to accurately knock down Pde4b expression in the AUD^{GABA}-S1Tr^{Sst} neural circuit and confirmed that reduction of Pde4b in the S1Tr^{Sst} neuron inputs from AUD^{GABA} improved anxiety-like behavior induced by acute stress. Surprisingly, our results revealed that knockdown of Pde4b expression in the AUD^{GABA}-S1Tr^{Sst} neural circuit improved the desensitization of neurons after acute stress. Given that cAMP signaling can activate PKA to enhance intracellular calcium concentrations and calcium influx, it is plausible that acute stress increased the expression of the Pde4b protein within S1Tr^{Sst} neurons, leading to decreased content of cAMP within these neurons. When the AUD^{GABA} neurons activated by acute stress released neurotransmitters onto S1Tr^{Sst} neurons, the weakened cAMP signaling pathway disrupted the equilibrium between the circuit, resulting in hypoactivity of S1Tr^{Sst} neurons during subsequent behavioral tests and giving rise to anxiety.

In conclusion, to our best knowledge, we offered the first evidence that acute stress could activate S1Tr^{Sst} neurons, causing

them to produce hypoactivity effects during the subsequent anxiety-like behavior test, ultimately resulting in anxiety-like behavior. We also provided a serial line of evidence that the S1Tr^{Sst} neurons involved in acute-stress-induced anxiety received inputs from GABAergic inhibitory neurons in the AUD. Finally, we indicated upregulation of several PDEs in the AUD^{GABA}-S1Tr^{Sst} neural circuit following acute stress, resulting in decreased activity of the cAMP signaling pathway so that decreasing Pde4b protein in the S1Tr^{Sst} neuron inputs from AUD^{GABA} could reverse anxiety-like behavior and neuronal desensitization induced by acute stress. In short, our study provides novel insights into the neural circuit and molecular mechanisms underlying acute stress-elicited anxiety.

Limitations of the study

In this study, our results revealed that Sst neurons activated by acute stress exhibited hypoactivity effects during the anxiety-like behavior test. However, it remains unclear whether the opto-/chemogenetic manipulations truly recapitulate the “desensitization” firing profile of the Sst cells through our manipulation approaches. Moreover, although we discovered that the expression of genes such as Pde4b increased after acute stress through spatial transcriptomics in the S1Tr, we were unable to precisely validate the elevated levels of Pde4b in the AUD^{GABA}-S1Tr^{Sst} neural circuit using western blot due to the lack of effective technical approaches. Finally, although we found that the cAMP levels in S1Tr decreased after acute stress, we were unable to more precisely verify whether the cAMP expression decreased in S1Tr^{Sst} neurons innervated by AUD^{GABA} at the circuit level or whether cAMP changed in S1Tr^{Sst} neuron input from AUD^{GABA} after Pde4b was knocked down.

RESOURCE AVAILABILITY

Lead contact

Further information and requests for resources and reagents should be directed to and will be fulfilled by the lead contact, Xu-Feng Xu (xuxufeng@qdu.edu.cn).

Materials availability

This study did not generate new unique reagents.

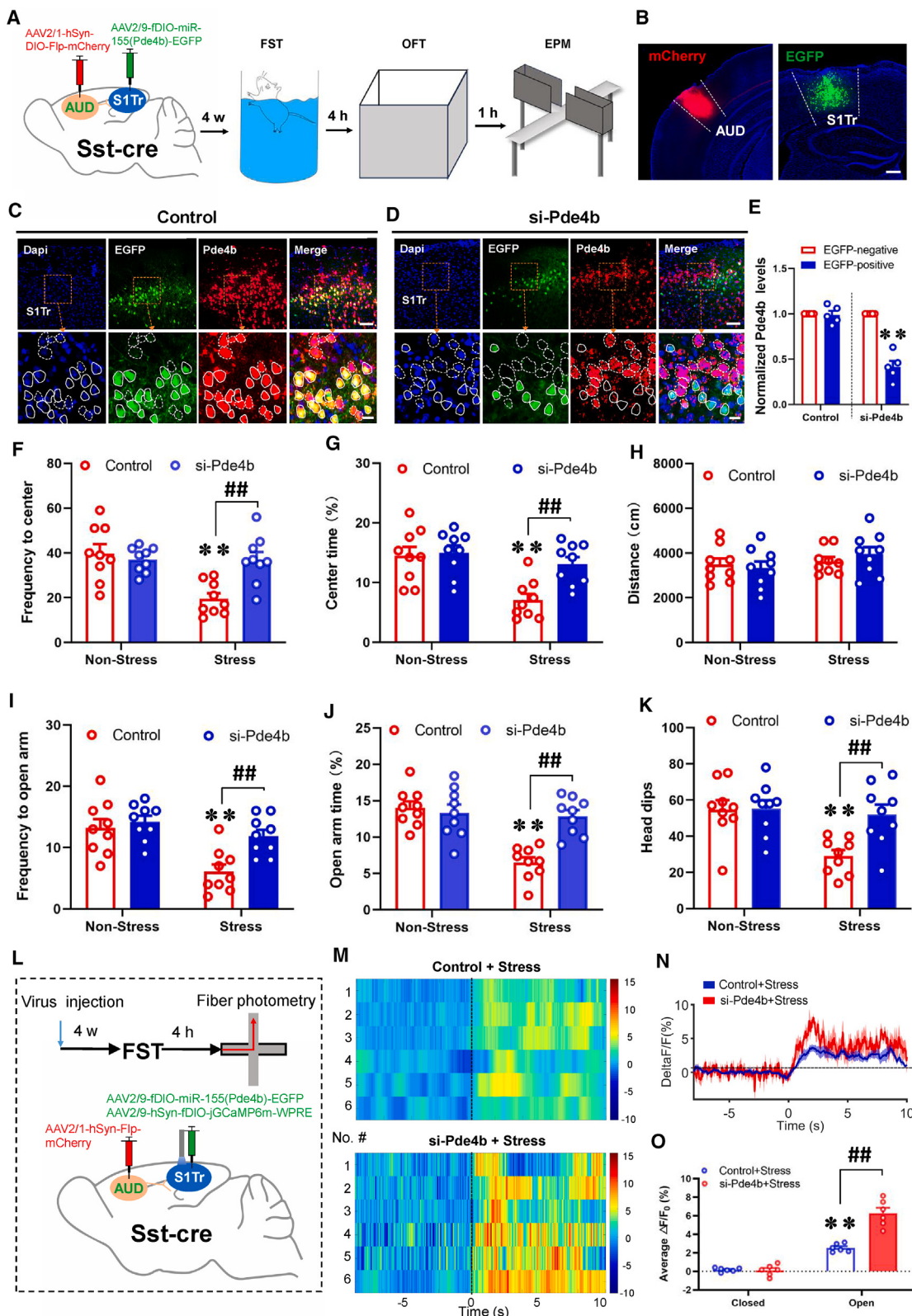
Data and code availability

- (1) The single-cell RNA-sequencing and spatial transcriptome sequencing data generated as parts of this study are publicly available at the Gene Expression Omnibus (GEO: GSE285495; and GSE285650).
- (2) All code used in this study has been previously published, and the pipelines are described in [STAR Methods](#).
- (3) Any additional information required to reanalyze the data reported in this paper is available from the [lead contact](#) upon request.

ACKNOWLEDGMENTS

This study was supported by the Shandong Province Natural Science Foundation (ZR2024MH063), the Major Program of Technological Innovation 2030 “Brain Science and Brain-inspired Research” (2021ZD0203002), the

stress: $F_{(1,44)} = 16.57, p = 0.0002$; hM4Di: $F_{(1,44)} = 7.227, p = 0.0101$; interaction: $F_{(1,44)} = 5.310, p = 0.0260$. I: stress: $F_{(1,44)} = 17.08, p = 0.0002$; hM4Di: $F_{(1,44)} = 6.241, p = 0.0163$; interaction: $F_{(1,44)} = 8.097, p = 0.0067$. J: stress: $F_{(1,44)} = 5.573, p = 0.0227$; hM4Di: $F_{(1,44)} = 2.907, p = 0.0952$; interaction: $F_{(1,44)} = 8.326, p = 0.0060$.



(legend on next page)

key project of the National Natural Science Foundation of China (81830035), the major program of National Natural Science Foundation of China (82090033), the program of the National Natural Science Foundation of China (32371187 and 32000788), the major basic research program of Shandong Province Natural Science Foundation (ZR2019ZD35), a Shandong Taishan Scholar Award, and the Fundamental Research Funds of Qingdao University.

AUTHOR CONTRIBUTIONS

Z.-X.X., X.-Y.W., N.Z., X.-T.Y., X.-Q.Z., Q.-L.W., and Z.L. performed the research; X.-F.X. analyzed data; and X.-F.X. conceived the project and wrote the manuscript with the help of X.Z. and H.-M.X.

DECLARATION OF INTERESTS

None of the authors has a conflict of interest to declare in relation to the present research.

STAR METHODS

Detailed methods are provided in the online version of this paper and include the following:

- KEY RESOURCES TABLE
- EXPERIMENTAL MODEL AND STUDY PARTICIPANT DETAILS
- METHOD DETAILS
 - Behavioral tests
 - Stereotactic surgery
 - Fiber photometry
 - Optogenetic experiments
 - Chemogenetic experiments
 - Neuronal apoptosis experiment
 - Pde4b gene knockdown
 - Cell cultures and transfection
 - Western blot
 - RT-PCR
 - Single-cell sequencing
 - Spatial transcriptome sequencing
 - RNAscope *in situ* hybridization
 - Determination of cAMP concentration
 - *In vitro* electrophysiology
 - Immunofluorescence staining
 - Neuroanatomical tract-tracing experiments
- QUANTIFICATION AND STATISTICAL ANALYSIS

Figure 7. Knockdown of Pde4b in AUD^{GABA}-S1Tr^{Sst} neural circuit relieves acute-stress-elicited anxiety and neuronal desensitization

(A) Experimental schedule for virus injection and subsequent behavioral tests.

(B) Frontal sections show mCherry-labeled cells in AUD and EGFP-labeled neurons in S1Tr. Scale bar, 200 μm.

(C-E) Representative pictures of RNAscope study show the effective knockdown of the expression of Pde4b by si-Pde4b virus. Solid coils indicate neurons infected with AAV viruses, while dotted coils indicate neighboring uninfected neurons. Scale bars, 100 μm (top) and 20 μm (bottom).

(F-H) The entries into the center zone (F), time spent in the center zone (G), and total distance traveled (H) in OFT.

(I-K) The entries into the open arm (I), time spent in the open arm (J), and head-dip times (K) in EPM.

(L) Experimental scheme of virus injection and fiber photometry tests.

(M) Examples of *in vivo* fluorescence changes of S1Tr^{Sst} neurons during EPM behavior test in control + stress (top) and si-Pde4b + stress (bottom) groups.

(N) Dynamics of GCamp6 signal 8 s before and 10 s after the mice enter EPM center and open arms.

(O) Statistics of the average Ca²⁺ fluorescence signaling changes in the closed and open arms of the EPM between mice in control + stress and si-Pde4b + stress groups.

All values are presented as the mean ± SEM. ***p* < 0.01 vs. EGFP-negative, two-tailed t test (E). ***p* < 0.01 vs. control group; ##*p* < 0.01, Bonferroni post hoc test after two-way ANOVA (F: stress: $F_{(1,32)} = 10.86, p = 0.0024$; si-Pde4b: $F_{(1,32)} = 5.588, p = 0.0243$; interaction: $F_{(1,32)} = 10.39, p = 0.0029$. G: stress: $F_{(1,32)} = 13.96, p = 0.0007$; si-Pde4b: $F_{(1,32)} = 6.958, p = 0.0128$; interaction: $F_{(1,32)} = 4.941, p = 0.0334$. H: stress: $F_{(1,32)} = 2.020, p = 0.1649$; si-Pde4b: $F_{(1,32)} = 0.08583, p = 0.7714$; interaction: $F_{(1,32)} = 0.8242, p = 0.3708$. I: stress: $F_{(1,32)} = 16.26, p = 0.0003$; si-Pde4b: $F_{(1,32)} = 8.376, p = 0.0068$; interaction: $F_{(1,32)} = 4.162, p = 0.0497$. J: stress: $F_{(1,32)} = 19.69, p = 0.0004$; si-Pde4b: $F_{(1,32)} = 9.885, p = 0.0036$; interaction: $F_{(1,32)} = 15.33, p = 0.0004$. K: stress: $F_{(1,32)} = 9.063, p = 0.0051$; si-Pde4b: $F_{(1,32)} = 5.913, p = 0.0208$; interaction: $F_{(1,32)} = 5.471, p = 0.0257$. O: arm: $F_{(1,20)} = 108.8, p < 0.0001$; si-Pde4b: $F_{(1,20)} = 20.44, p < 0.0001$; interaction: $F_{(1,20)} = 33.22, p < 0.0001$.

SUPPLEMENTAL INFORMATION

Supplemental information can be found online at <https://doi.org/10.1016/j.celrep.2025.115253>.

Received: June 19, 2024

Revised: December 11, 2024

Accepted: January 10, 2025

Published: January 30, 2025

REFERENCES

1. Dean, E. (2016). Anxiety. Nurs. Stand. 30, 15. <https://doi.org/10.7748/ns.30.46.15.s17>.
2. Kraeuter, A.K., Guest, P.C., and Sarnyai, Z. (2019). The Elevated Plus Maze Test for Measuring Anxiety-Like Behavior in Rodents. Methods Mol. Biol. 1916, 69–74. https://doi.org/10.1007/978-1-4939-8994-2_4.
3. Komada, M., Takao, K., and Miyakawa, T. (2008). Elevated plus maze for mice. J. Vis. Exp. 1088. <https://doi.org/10.3791/1088>.
4. Kraeuter, A.K., Guest, P.C., and Sarnyai, Z. (2019). The Open Field Test for Measuring Locomotor Activity and Anxiety-Like Behavior. Methods Mol. Biol. 1916, 99–103. https://doi.org/10.1007/978-1-4939-8994-2_9.
5. Chen, Y.H., Wu, J.L., Hu, N.Y., Zhuang, J.P., Li, W.P., Zhang, S.R., Li, X.W., Yang, J.M., and Gao, T.M. (2021). Distinct projections from the infralimbic cortex exert opposing effects in modulating anxiety and fear. J. Clin. Invest. 131, e145692. <https://doi.org/10.1172/JCI145692>.
6. Morel, C., Montgomery, S.E., Li, L., Durand-de Cuttoli, R., Teichman, E.M., Juarez, B., Tzavaras, N., Ku, S.M., Flanigan, M.E., Cai, M., et al. (2022). Midbrain projection to the basolateral amygdala encodes anxiety-like but not depression-like behaviors. Nat. Commun. 13, 1532. <https://doi.org/10.1038/s41467-022-29155-1>.
7. Jimenez, J.C., Su, K., Goldberg, A.R., Luna, V.M., Biane, J.S., Ordek, G., Zhou, P., Ong, S.K., Wright, M.A., Zweifel, L., et al. (2018). Anxiety Cells in a Hippocampal-Hypothalamic Circuit. Neuron 97, 670–683.e6. <https://doi.org/10.1016/j.neuron.2018.01.016>.
8. Qi, G., Zhang, P., Li, T., Li, M., Zhang, Q., He, F., Zhang, L., Cai, H., Lv, X., Qiao, H., et al. (2022). NAc-VTA circuit underlies emotional stress-induced anxiety-like behavior in the three-chamber vicarious social defeat stress mouse model. Nat. Commun. 13, 577. <https://doi.org/10.1038/s41467-022-28190-2>.
9. Tye, K.M., Prakash, R., Kim, S.Y., Feno, L.E., Grosenick, L., Zarabi, H., Thompson, K.R., Grardinari, V., Ramakrishnan, C., and Deisseroth, K. (2011). Amygdala circuitry mediating reversible and bidirectional control of anxiety. Nature 471, 358–362. <https://doi.org/10.1038/nature09820>.

10. Wang, D., Pan, X., Zhou, Y., Wu, Z., Ren, K., Liu, H., Huang, C., Yu, Y., He, T., Zhang, X., et al. (2023). Lateral septum-lateral hypothalamus circuit dysfunction in comorbid pain and anxiety. *Mol. Psychiatry* 28, 1090–1100. <https://doi.org/10.1038/s41380-022-01922-y>.
11. Wang, X., Zhang, Y., Wang, X., Dai, J., Hua, R., Zeng, S., and Li, H. (2020). Anxiety-related cell-type-specific neural circuits in the anterior-dorsal bed nucleus of the stria terminalis. *Sci. Bull.* 65, 1203–1216. <https://doi.org/10.1016/j.scib.2020.03.028>.
12. Jin, Y., Meng, Q., Mei, L., Zhou, W., Zhu, X., Mao, Y., Xie, W., Zhang, X., Luo, M.H., Tao, W., et al. (2020). A somatosensory cortex input to the caudal dorsolateral striatum controls comorbid anxiety in persistent pain. *Pain* 161, 416–428. <https://doi.org/10.1097/j.pain.0000000000001724>.
13. Ishikawa, T., Murata, K., Okuda, H., Potapenko, I., Hori, K., Furuyama, T., Yamamoto, R., Ono, M., Kato, N., Fukazawa, Y., and Ozaki, N. (2023). Pain-related neuronal ensembles in the primary somatosensory cortex contribute to hyperalgesia and anxiety. *iScience* 26, 106332. <https://doi.org/10.1016/j.isci.2023.106332>.
14. Kropf, E., Syan, S.K., Minuzzi, L., and Frey, B.N. (2019). From anatomy to function: the role of the somatosensory cortex in emotional regulation. *Braz. J. Psychiatry* 41, 261–269. <https://doi.org/10.1590/1516-4446-2018-0183>.
15. Canavero, S., and Bonicalzi, V. (2013). Role of primary somatosensory cortex in the coding of pain. *Pain* 154, 1156–1158. <https://doi.org/10.1016/j.pain.2013.02.032>.
16. Varlinskaya, E.I., Johnson, J.M., Przybysz, K.R., Deak, T., and Diaz, M.R. (2020). Adolescent forced swim stress increases social anxiety-like behaviors and alters kappa opioid receptor function in the basolateral amygdala of male rats. *Prog. Neuro-Psychopharmacol. Biol. Psychiatry* 98, 109812. <https://doi.org/10.1016/j.pnpbp.2019.109812>.
17. Chen, D., Lou, Q., Song, X.J., Kang, F., Liu, A., Zheng, C., Li, Y., Wang, D., Qun, S., Zhang, Z., et al. (2024). Microglia govern the extinction of acute stress-induced anxiety-like behaviors in male mice. *Nat. Commun.* 15, 449. <https://doi.org/10.1038/s41467-024-44704-6>.
18. Zhang, N., Zhao, S., Ma, Y., Xiao, Z., Xue, B., Dong, Y., Wang, Q., Xu, H., Zhang, X., and Wang, Y. (2024). Hyperexcitation of ovBNST CRF neurons during stress contributes to female-biased expression of anxiety-like avoidance behaviors. *Sci. Adv.* 10, eadk7636. <https://doi.org/10.1126/sciadv.adk7636>.
19. Taniguchi, H., He, M., Wu, P., Kim, S., Paik, R., Sugino, K., Kvitsiani, D., Fu, Y., Lu, J., Lin, Y., et al. (2011). A resource of Cre driver lines for genetic targeting of GABAergic neurons in cerebral cortex. *Neuron* 71, 995–1013. <https://doi.org/10.1016/j.neuron.2011.07.026>.
20. Wickersham, I.R., Finke, S., Conzelmann, K.K., and Callaway, E.M. (2007). Retrograde neuronal tracing with a deletion-mutant rabies virus. *Nat. Methods* 4, 47–49. <https://doi.org/10.1038/nmeth999>.
21. Sun, Y., Nguyen, A.Q., Nguyen, J.P., Le, L., Saur, D., Choi, J., Callaway, E.M., and Xu, X. (2014). Cell-type-specific circuit connectivity of hippocampal CA1 revealed through Cre-dependent rabies tracing. *Cell Rep.* 7, 269–280. <https://doi.org/10.1016/j.celrep.2014.02.030>.
22. Zingg, B., Chou, X.L., Zhang, Z.G., Mesik, L., Liang, F., Tao, H.W., and Zhang, L.I. (2017). AAV-Mediated Anterograde Transsynaptic Tagging: Mapping Corticocollicular Input-Defined Neural Pathways for Defense Behaviors. *Neuron* 93, 33–47. <https://doi.org/10.1016/j.neuron.2016.11.045>.
23. Conti, M., and Beavo, J. (2007). Biochemistry and physiology of cyclic nucleotide phosphodiesterases: essential components in cyclic nucleotide signaling. *Annu. Rev. Biochem.* 76, 481–511. <https://doi.org/10.1146/annurev.biochem.76.060305.150444>.
24. Plattner, F., Hayashi, K., Hernández, A., Benavides, D.R., Tassin, T.C., Tan, C., Day, J., Fina, M.W., Yuen, E.Y., Yan, Z., et al. (2015). The role of ventral striatal cAMP signaling in stress-induced behaviors. *Nat. Neurosci.* 18, 1094–1100. <https://doi.org/10.1038/nn.4066>.
25. Zhang, Y., Lu, W., Wang, Z., Zhang, R., Xie, Y., Guo, S., Jiao, L., Hong, Y., Di, Z., Wang, G., and Aa, J. (2020). Reduced Neuronal cAMP in the Nucleus Accumbens Damages Blood-Brain Barrier Integrity and Promotes Stress Vulnerability. *Biol. Psychiatry* 87, 526–537. <https://doi.org/10.1016/j.biopsych.2019.09.027>.
26. Murphy, J.G., Sanderson, J.L., Gorski, J.A., Scott, J.D., Catterall, W.A., Sather, W.A., and Dell'Acqua, M.L. (2014). AKAP-anchored PKA maintains neuronal L-type calcium channel activity and NFAT transcriptional signaling. *Cell Rep.* 7, 1577–1588. <https://doi.org/10.1016/j.celrep.2014.04.027>.
27. Ghirardi, M., Benfenati, F., Giovedì, S., Fiumara, F., Milanese, C., and Montarolo, P.G. (2004). Inhibition of neurotransmitter release by a nonphysiological target requires protein synthesis and involves cAMP-dependent and mitogen-activated protein kinases. *J. Neurosci.* 24, 5054–5062. <https://doi.org/10.1523/JNEUROSCI.5671-03.2004>.
28. Tame, L., Braun, C., Holmes, N.P., Farne, A., and Pavani, F. (2016). Bilateral representations of touch in the primary somatosensory cortex. *Cogn. Neuropsychol.* 33, 48–66. <https://doi.org/10.1080/02643294.2016.1159547>.
29. Kim, W., Kim, S.K., and Nabekura, J. (2017). Functional and structural plasticity in the primary somatosensory cortex associated with chronic pain. *J. Neurochem.* 141, 499–506. <https://doi.org/10.1111/jnc.14012>.
30. Misrani, A., Tabassum, S., Wang, T., Huang, H., Jiang, J., Diao, H., Zhao, Y., Huang, Z., Tan, S., Long, C., and Yang, L. (2024). Vibration-reduced anxiety-like behavior relies on ameliorating abnormalities of the somatosensory cortex and medial prefrontal cortex. *Neural Regen. Res.* 19, 1351–1359. <https://doi.org/10.4103/1673-5374.385840>.
31. Cook, J.R., Li, H., Nguyen, B., Huang, H.H., Mahdavian, P., Kirchgessner, M.A., Strassmann, P., Engelhardt, M., Callaway, E.M., and Jin, X. (2022). Secondary auditory cortex mediates a sensorimotor mechanism for action timing. *Nat. Neurosci.* 25, 330–344. <https://doi.org/10.1038/s41593-022-01025-5>.
32. Barr, H.J., Wall, E.M., and Woolley, S.C. (2021). Dopamine in the songbird auditory cortex shapes auditory preference. *Curr. Biol.* 31, 4547–4559.e5. <https://doi.org/10.1016/j.cub.2021.08.005>.
33. Ricciarelli, R., and Fedele, E. (2018). cAMP, cGMP and Amyloid beta: Three Ideal Partners for Memory Formation. *Trends Neurosci.* 41, 255–266. <https://doi.org/10.1016/j.tins.2018.02.001>.
34. Gabellini, N. (2004). Transcriptional regulation by cAMP and Ca²⁺ links the Na⁺/Ca²⁺ exchanger 3 to memory and sensory pathways. *Mol. Neurobiol.* 30, 91–116. <https://doi.org/10.1385/MN:30:1:091>.
35. Zhang, H., Kong, Q., Wang, J., Jiang, Y., and Hua, H. (2020). Complex roles of cAMP-PKA-CREB signaling in cancer. *Exp. Hematol. Oncol.* 9, 32. <https://doi.org/10.1186/s40164-020-00191-1>.
36. Gao, F., Yang, S., Wang, J., and Zhu, G. (2022). cAMP-PKA cascade: An outdated topic for depression? *Biomed. Pharmacother.* 150, 113030. <https://doi.org/10.1016/j.biopha.2022.113030>.

STAR★METHODS

KEY RESOURCES TABLE

REAGENT or RESOURCE	SOURCE	IDENTIFIER
Antibodies		
Rabbit anti-Pde4b antibody	Cell Signaling Technology	Cat# 72096, RRID:AB_2799812
Mouse anti- α -tubulin antibody	Sigma- Aldrich	Cat# T6199, RRID:AB_477583
Goat anti-mouse secondary antibody	Merck	Cat# AP124P, RRID:AB_90456
Goat anti-rabbit secondary antibody	Merck	Cat# 12-348, RRID:AB_390191
Rabbit anti-c-Fos	Abcam	Cat# ab190289, RRID:AB_2737414
Goat anti-rabbit AlexaFluor-488/555	Invitrogen	Cat#A-11034/A-21429; RRID : AB_2576217, RRID : AB_2535850
Goat anti-mouse AlexaFluor-488/555	Invitrogen	Cat#A-21206/A-21424; RRID : AB_2535792, RRID : AB_141780
Bacterial and virus strains		
AAV2/9-hSyn-DIO-jGCaMP6m	OBio technology	N/A
AAV2/9-hSyn-DIO-EGFP	OBio technology	N/A
AAV2/9-hSyn-DIO-eNpHR3.0-mCherry	OBio technology	N/A
AAV2/9-hSyn-DIO-mCherry	OBio technology	N/A
AAV2/9-hSyn-DIO-ChR2-EGFP	OBio technology	N/A
AAV2/9-EF1a-fDIO-eNpHR3.0-mCherry	OBio technology	N/A
AAV2/9-EF1a-fDIO-mCherry	OBio technology	N/A
AAV2/9-hSyn-DIO-hM4Di-mCherry	OBio technology	N/A
AAV2/9-hSyn-DIO-hM3Dq-mCherry	OBio technology	N/A
AAV/Retro-hSyn-Cre-mCherry	OBio technology	N/A
AAV2/9-VGAT-DIO-hM4Di-EGFP	OBio technology	N/A
AAV2/9-VGAT-DIO-EGFP	OBio technology	N/A
AAV2/9-hSyn-DIO-Caspase3-EGFP	OBio technology	N/A
AAV2/1-hSyn-DIO-Flp-mCherry	GeneChem.	N/A
AAV2/9-CMV-fDIO-miR-155(Pde4b)-EGFP	GeneChem.	N/A
AAV2/9-CMV-fDIO-EGFP	GeneChem.	N/A
AAV2/1-hSyn-DIO-Flp-EGFP	OBio technology	N/A
AAV2/9-DIO-RVG	OBio technology	N/A
AAV2/9-DIO-EGFP-TVA	BrainVTA	N/A
RV-Enva-ΔG-mCherry	BrainVTA	N/A
Chemicals, peptides, and recombinant proteins		
Clozapine N-oxide	Cayman Chemical, USA	Cat#16882
Phosphate Buffer Saline	Solarbio	Cat#P1010
Paraformaldehyde	Sigma	Cat#441244
Pierce ECL	Thermo Fisher Scientific	Cat#32209
Mm-Slc32a1-C2	ACD Bio	Cat #319191-C2
Mm-Slc17a7-C3	ACD Bio	Cat #416631-C3
Mm-Pde4b-C1	ACD Bio	Cat #577191-C1
Mm-Sst-C1	ACD Bio	Cat #404631-C1
OCT	Sakura	Cat #4583
DMEM/F-12	Invitrogen	Cat#11320033
B27	Invitrogen	Cat#17504044
trypsin-EDTA	Invitrogen	Cat#27250018
DAPI	Sigma	Cat#D9542
poly-d-lysine	Gibco	Cat#A3890401

(Continued on next page)

Continued

REAGENT or RESOURCE	SOURCE	IDENTIFIER
Neurobasal	Gibco	Cat#21103049
fetal bovine serum	Gibco	Cat#A5670801
Critical commercial assays		
ReverTra Ace qPCR RT Kit	Toyobo, Osaka	Cat#FSQ-101
cAMP Direct ELISA Immunoassay Kit	Abcam	Cat#ab138880
Deposited data		
Data files for S1Tr scRNA-seq	This paper	GSE285495
Data files for S1Tr spatial transcriptome sequencing	This paper	GSE285650
Experimental models: Organisms/strains		
C57BL/6J	Beijing Vital River Laboratory Animal Technology Co., Ltd.	219
Sst-Cre mice	Suzhou Geneandpeace Biotechnology company Co., Ltd.	JAX: 028864
Oligonucleotides		
The Pde4b primer sequences forward 5'-GAGCTACACAGCACCTGTTAT-3'	Takara	N/A
The Pde4b primer sequences reverse 5'-GGAAGAGAGGGAAAGTGTAGTG-3'	Takara	N/A
Sst-cre Tg Mutant Forward 5'TCAGGTACATGGATCCACTAGTTCT-3'	Jackson laboratories	Primer 53428
Sst-cre WT allele Wildtype Forward 5'-GAGGTCTGCCAACTCGAAC-3'	Jackson laboratories	Primer 53429
Sst-cre Tg allele Common 5'-AGTCAAACGTTGCTCTTCA-3'	Jackson laboratories	Primer 53430
Software and algorithms		
View Point Life Sciences	Montreal, QC, Canada	N/A
Etho Vision software	Noldus Information Technology	N/A
Matlab	MathWorks	N/A
OLYMPUS FV3000 system	OLYMPUS	N/A
digital pathology section system	OLYMPUS	N/A
GraphPad Prism 9	GraphPad Software	N/A
EndNote X9	Thomson ResearchSoft	N/A
Other		
Lasers for optogenetics	ThinkerTech	N/A
Fiber	Inper	N/A

EXPERIMENTAL MODEL AND STUDY PARTICIPANT DETAILS

C57BL/6J pregnant female mice used for primary culture and C57BL/6J male mice (2-3 months old) were obtained from the Vital River Laboratory Animal Technology Co., Ltd (Beijing, China). Sst male Cre-recombinase mice (Sst-Cre mice, strain No.028864) were purchased from Geneandpeace Biotechnology company Co., Ltd (Suzhou, China) and genotyped based on the protocol of Jackson Laboratories. All mice were raised in standard mice cages of a temperature controlled room ($22 \pm 2^\circ\text{C}$), and freely obtained food and water under diurnal condition (12 hours of light/dark cycle). The use and care of mice were approved by the Animal Ethics and Experimentation Committee of the Qingdao University.

METHOD DETAILS

Behavioral tests

Behavioral testing was performed during the light phase of the 9:00 A.M. to 4:00 P.M cycle. Before testing, mice were allowed to acclimate to the testing chamber for 2 hours.

Forced-swimming test

Mice were placed in a 65×30 cm organic glass cylinder (filled with 25°C water at a height of 10 cm) for 10 minutes. An automated behavioral tracking system (View Point Life Sciences, Montreal, QC, Canada) were used to quantify the duration of immobility.

Acute restraint stress

The Sst-Cre and C57BL/6 mice were randomly divided into stressed group and non-stressed group. The stressed group underwent restraint stress during the time of 9:00 A.M.–11:00 A.M. For restraint stress, mice were confined to well-ventilated polypropylene restrainers for 2 hours without access to water and food. All mice were sent back to the home cage at the end of the stress phase. The non-stressed mice were handled for 2 minutes and then sent back to the home cage.

Open field test

OFT testing was measured in a device ($40 \times 40 \times 35$ cm, centered in a 20×20 cm square) equipped with 12×12 photobeam arrays in a dimly lit room. The light intensity in the center zone of open field was ~ 10 lux. At the beginning of the experiment, mice were placed in the center of the open field and allowed to move freely for 9 minutes. All behaviors were recorded on video and data were analyzed using Etho Vision software (Noldus Information Technology).

Elevated plus maze

Anxiety levels were measured in an elevated plus maze (55 cm above the ground) with two opposing open arms (30×8 cm) and two opposing closed arms ($30 \times 8 \times 15$ cm). The light intensity in the central region of the EPM was ~ 15 lux. At the beginning of the experiment, mice were first put in the center zone of the EPM with its head toward an open arm, and allowed to explore freely for 9 minutes. All behaviors were recorded on video and data were analyzed using Etho Vision software (Noldus Information Technology).

Stereotactic surgery

For stereotactic experiments, the adult mice with isoflurane anesthesia (5% for induction, 1.5% for maintenance) were set in the stereotactic apparatus (8001, RWD Life Science) before the surgery. An incision was first made below the midline of the scalp, followed by a stereotactic ally drilled holes over the skull. For virus administration, a glass micropipette controlled by a syringe pump was used to microinject the virus into the target area at a rate of 30 nl/min. After completion of virus injection, the syringe continued to remain in place for 10 minutes and then slowly withdrawn the microtubule.

Fiber photometry

Adult male Sst-Cre mice under anesthesia with isoflurane received a microinjection of AAV2/9-hSyn-DIO-jGCaMP6m (or AAV2/9-hSyn-DIO-EGFP as controls; 0.1 ml, titer 10^{12} particles per ml; OBio technology, Shanghai, China) into the S1Tr (AP -1.60 mm, ML ± 1.70 mm, DV -0.75 mm) and then ipsilaterally implanted a photometry fiber 100 mm above the S1Tr. Four weeks later, the photometry signal data was collected during EPM test. All the trials were conducted until the photometry signal was stable. For analysis, Matlab was used to convert the photometry signal F to $\Delta F/F$ as following formula. The photometry signals during the stress experiences were matched with video recordings.

Optogenetic experiments

Adult Sst-Cre mice under anesthesia with isoflurane received microinjections of the following viruses (0.1 μ l, titer 10^{12} particles per ml) at a speed of 30 nl/min in different experiments: (1) AAV2/9-hSyn-DIO-eNpHR3.0-mCherry (AAV2/9-hSyn-DIO-mCherry as control; purchased from OBio technology, Shanghai, China) or AAV2/9-hSyn-DIO-ChR2-EGFP (AAV2/9-hSyn-DIO-EGFP as control; OBio technology, Shanghai, China) into the bilateral S1Tr (AP -1.60 mm, ML ± 1.70 mm, DV -0.75 mm); (2) AAV2/1-hSyn-DIO-Flp-EGFP (OBio technology, Shanghai, China) into bilateral AUD (AP -2.70 mm, ML ± 3.70 mm, DV -1.90 mm), VO (AP $+2.46$ mm, ML ± 0.75 mm, DV -2.50 mm) or M2 (AP $+0.98$ mm, ML ± 0.70 mm, DV -1.25 mm), followed by AAV2/9-EF1a-fDIO-eNpHR3.0-mCherry (AAV2/9-EF1a-fDIO-mCherry as control; OBio technology, Shanghai, China) into bilateral S1Tr (AP -1.60 mm, ML ± 1.70 mm, DV -0.75 mm). After virus injection, the optical fiber housing units were implanted above the bilateral S1Tr and secured. Four weeks later, mice received FST stress, and 4 hours later the fiber patch wire assembled with a standard kit was attached to the optic fiber. Yellow laser (594 nm wavelength) or blue laser (450 nm wavelength) was delivered to S1Tr by a TTL controlled laser (Thinker Tech Nanjing BioScience Inc., Nanjing, China) with adjustable output intensity via the optic fiber patch cord-optic fiber implant system (Plastic One, Canada). For blue light photoactivation, each mouse received 10 Hz stimuli for 3 min during OFT and EPM. For opto-suppression experiments, mice received 200 ms yellow light illumination (5 mW, 3 Hz) for 3 minutes during OFT and EPM.

Chemogenetic experiments

For chemogenetic strategies on Sst-Cre mice, AAV2/9-hSyn-DIO-hM4Di-mCherry (AAV2/9-hSyn-DIO-mCherry as control; purchased from OBio technology, Shanghai, China) or AAV2/9-hSyn-DIO-hM3Dq-mCherry (AAV2/9-hSyn-DIO-mCherry as control; OBio technology, Shanghai, China) into the bilateral S1Tr. C57BL/6 mice received an injection of AAV/Retro-hSyn-Cre-mCherry into bilateral S1Tr, followed by an injection of AAV2/9-VGAT-DIO-hM4Di-EGFP (AAV2/9-VGAT-DIO-EGFP as control) into bilateral AUD. Four weeks after the virus injection, CNO or vehicle was injected into mice (0.5 mg/kg, i.p.; Cayman Chemical, USA), followed by behavioral experiments 30 minutes later.

Neuronal apoptosis experiment

For Neuronal apoptosis strategy on Sst-Cre mice, AAV2/9-hSyn-DIO-Caspase3-EGFP (AAV2/9-hSyn-DIO-EGFP as control; purchased from OBIO technology, Shanghai, China) into the bilateral S1Tr. Behavioral experiments were conducted four weeks after the virus injection.

Pde4b gene knockdown

Design of Pde4b knockdown AAV viruses

The construction plasmid vectors of Pde4b gene knockdown and the location of the insertion sequence are shown in [Figure S11A](#) of the supplementary figures. miR155 mediated RNA interference (RNAi) methods were used to knockdown Pde4b mRNA. Three RNAi sequences for Pde4b were designed to jointly knock down the Pde4b mRNA. The three RNAi sequences we used are shown in [Figure S11B](#) in the supplementary figures. Plasmid construction, AAV virus packaging, and titer detection were all performed by GeneChem. Co., Ltd.

Application of Pde4 knockdown AAV viruses

Sst-Cre mice under anesthesia with isoflurane received microinjections of the following viruses (0.1 ml, titer 10^{12} particles per ml) at a speed of 30 nl/min: AAV2/1-hSyn-DIO-Flp-mCherry (GeneChem. Co., Ltd, Shanghai, China) into bilateral AUD, followed by an injection of AAV2/9-CMV-fDIO-miR-155(Pde4b)-EGFP (or AAV2/9-CMV-fDIO-EGFP as control; GeneChem. Co., Ltd, Shanghai, China) into bilateral S1Tr. Four weeks later, mice received FST stress, followed 4 hours later by behavioral tests.

Cell cultures and transfection

Brains of day 18 C57BL/6 mouse embryos were removed and then placed in Hank balanced salt solution at 4°C. Dissected the cerebral cortical tissue and digested with 1.5% trypsin-EDTA (Invitrogen) at 37°C for 10 minutes, and then terminated with a mixture of 10% fetal bovine serum (Gibco) plus DMEM/F-12 (1:1, Invitrogen). Inoculate neurons onto six-well plates precoated with 0.1 mg/mL poly-d-lysine in neurobasal medium (Gibco), and add 1 × B27 (Gibco) and 0.05 mM glutamine. Incubate primary cultured cortical neurons in saturated humidity, 5% CO₂, and constant temperature (37°C). Neurons were first cultured for three days and then AAV viruses were added to six-well plates to infect the neurons. Seven days later, proteins and RNA were extracted from neurons for subsequent analysis.

Western blot

After treating with Tris-HCl buffer with a pH value of 7.5, cells were lysed in RIPA buffer with ice-cold (3.8 µg/mL aprotinin, 1% NP-40, 150 mmol/L NaCl, 1 mmol/L EDTA, 1 µg/mL leupeptin, 1 µg/mL pepstatin, 1 mmol/L PMSF, 1 mmol/L Na₃VO₄, and 2 mmol/L NaF). The extracts were separated by centrifugation at 14000g for 20 minutes (4°C). Supernatants were gathered and washed with an SDS sample buffer, and SDS-PAGE was used to resolve the proteins. Mouse anti-α-tubulin (Sigma-Aldrich, Saint Louis, USA, T6199, 1:10000) and rabbit anti-Pde4b antibody (Cat. 720965, 1:1000; Cell Signaling Technology, USA) were separately used as primary antibodies. Goat anti-mouse or anti-rabbit secondary antibodies (Merck, Germany, 1:1000) were performed to react with the corresponding primary antibodies. The protein imaging was shown using an enhanced chemiluminescence system (Pierce ECL, Thermo Fisher Scientific, Waltham, USA). Quantity One (version 4.6.2, Bio-Rad, Hercules, USA) was used for data statistics of protein intensity.

RT-PCR

TRIzol-A+ RNA isolation (Tiangen, Beijing, China) reagent was used to isolate the total RNA according to the manufacturer's protocol. We treated 0.5 µg aliquot of each sample with DNase to avoid DNA contamination and then used the ReverTra Ace qPCR RT Kit (catalog #FSQ-101; Toyobo, Osaka, Japan) for reverse transcription. We performed quantitative real-time RT-PCR in a Cycler (Bio-Rad) with SYBR-Green (Roche, Basel, Switzerland). The Pde4b primer sequences: forward, GAGCTACACAGCACCTGTTAT; reverse, GGAAGAGAGGGAAAGTGTAGTG. We performed three assays for each sample and used $2^{-\Delta\Delta CT}$ to normalize the siRNA levels to the β-actin levels in each well.

Single-cell sequencing

Mice received forced swimming test, followed 30 minutes later by rapidly extracting the whole brains and placed on a precooled metal plate. Bilateral S1Tr were rapidly dissected according to anatomical landmarks. The S1Tr was defined as AP: -1.34 to -1.82 mm. We snap-frozen the fresh tissues in liquid nitrogen and stored at -80°C to preserve the samples. Single cell sequencing was performed using the 10 X Genomics, and Libraries were sequenced on the Illumina NovaSeq 6000 System at LC Bio Technology Co., Ltd. in Hangzhou, China. For cell clustering analysis, we first singled out all FBJ osteosarcoma oncogene (c-Fos) gene-expressing neurons and then divided them into Glutamatergic neurons group, GABAergic neurons group and other neurons group. Solute carrier family 17, member 7 (Slc17a7, which encodes vesicular glutamate transporter 1), was used as a marker of glutamatergic neurons; Glutamate decarboxylase 1 (Gad1, which encodes GAD67) was used as a marker of GABAergic neurons, and the remaining neurons were classified as other neurons. In the process of classifying GABAergic neurons, the mouse VIP gene was used as a marker for VIP neurons, the Pvalb gene as a marker for Pvalb neurons, the Sst gene as a marker for Sst neurons, and the remaining GABAergic neurons were classified as other neurons.

Spatial transcriptome sequencing

Adult Sst-Cre mice received microinjections of AAV2/1-hSyn-DIO-Flp-EGFP into bilateral AUD, followed by AAV2/9-EF1a-fDIO-eNpHR3.0-mCherry into bilateral S1Tr of Sst-Cre mice. Four weeks later, Mice received FST stress (non-stress mice as control), followed 2 hours later by rapidly extracting the whole brains and placed on a precooled metal plate. The parts containing the target brain regions in the control group and the experimental group were removed and placed together, embedded by optimal cutting temperature compound (OCT), and cut into the virus expression area by frozen section. The brain slices with a thickness of 10 μm were sectioned for spatial transcriptome sequencing, and multiple sections were obtained for RNA extraction using a nucleic acid extraction kit. The quality of the sample preparation was assessed by the RIN value. Fluorescence microscopy observation and H&E staining were conducted to observe the tissue morphology and locate the fluorescent spots. Only samples that satisfied both the condition of $\text{RIN} \geq 7$ and had complete histopathological information with significant mCherry fluorescence were eligible for subsequent experimental procedures. Taking the optimized time of permeabilization preexperiment as the condition, the capture labeling experiment was carried out on the formal experimental samples cut again, including a series of experimental processes such as tissue patch, fixation, H&E staining and imaging, tissue permeabilization, cDNA synthesis, cDNA amplification, and sequencing library construction. After the construction of the library is completed, quality control is conducted. After the quality inspection is qualified, sequencing is carried out on the machine. The 10x visium spatial transcriptome library was sequenced using the Illumina NovaSeq PE150 strategy at GeneChem. Co., Ltd, in Shanghai, China. To identify the spots containing AAV viruses, the exogenous element sequences fDIO, eNpHR3.0, mCherry and WPRE (all the way to polyA) of AAV2/9-EF1a-fDIO-eNpHR3.0-mCherry were added to the library for construction and analysis. The spots containing these genes were selected as mCherry positive neurons, and the rest were considered as mCherry negative neurons. We used the FindAllMarkers function to identify marker genes of each cluster. The differentially expressed genes (DEGs) of mCherry positive neurons in stressed mouse, compared with those in non-stressed mouse, were passing the statistical threshold of the log-fold-change > 0.25 and adjusted p value < 0.05 . Then, we used the R package ClusterProfiler to investigate a functional enrichment analysis of the DEGs. The DEGs were mapped to known sources of functional pathway (including pathways from KEGG and GO).

RNAscope *in situ* hybridization

In situ hybridization was performed to detect the Slc32a1 and Slc17a7 mRNA with the corresponding RNAscope probes (Mm-Slc32a1-C2, ACD Bio #319191-C2; Mm-Slc17a7-C3, ACD Bio #416631-C3; Mm-Sst-C1, ACD Bio #404631-C1; Mm-Pde4b-C1, ACD Bio #577191-C1). We eluted the brain sections (fixed with the 10% neutralized formalin) in PBS and put them on microscope slides, and then air-dried overnight at -20°C , followed by standard hybridization protocols described in the manufacturer's instructions. Confocal images were taken using an OLYMPUS FV3000 system.

Determination of cAMP concentration

Quantitative cAMP measurements were conducted on collected tissue samples (S1Tr) using the cAMP Direct ELISA Immunoassay Kit (Fluorometric) (Abcam, ab138880). Frozen tissue was weighed and 10 $\mu\text{L}/\text{mg}$ of Cell Lysis Buffer was added. The tissue was homogenized with a Dounce homogenizer for 10 – 15 passes on ice. The sample was centrifuged for 5 minutes at 4°C at top speed using a cold microcentrifuge to remove any insoluble material. The supernatant was collected and transferred to a new tube. 75 μL of standard and 7.5 μL of samples (the volume was adjusted to 75 $\mu\text{L}/\text{well}$ with Assay Buffer) were added to the wells of the anti-cAMP coated 96-well plate. HRP-cAMP was added to each standard and sample well and incubated for 2 hours, followed by extensive washing. Detector AbRed, a fluorophore capable of reacting with HRP-cAMP, was added to each well and incubated. Fluorescence was monitored (Ex. 540 nm, Em. 590 nm). A standard curve was performed daily within a range of 0.3 nM to 100 nM cAMP.

In vitro electrophysiology

We removed the mouse brain, cut 300 μm coronal brain vibrisections and maintained them in the artificial cerebral spinal fluid saturated with 95% O_2 -5% CO_2 (ACSF: 1.25 mM KH₂PO₄, 25 mM NaHCO₃, 1.25 mM KCl, 125 mM NaCl, 1 mM CaCl₂, 1.5 mM MgCl₂, and 16 mM glucose). The patch pipettes contained an intracellular solution (20 mM KCl, 120 mM K gluconate, 10 mM phosphocreatine Na salt, 10 mM HEPES, 2 mM MgCl₂, 2 mM ATP Na salt, 0.4 mM GTP Na salt, pH 7.35). To distinguish the electrical fingerprints of the S1Tr neurons which expressing mCherry, neurons were visually discriminated using a fluorescent microscope and current clamped at -51 mV.

Immunofluorescence staining

After FST stress, the brains were extracted and fixed in 4% paraformaldehyde (PFA) for 24 hours, and then immersed in 30% sucrose at 4°C . We sectioned and collected the brain slices at 40 μm using a freezing microtome. The brain slices were eluted three times in PBS for 10 minutes, and then incubated in blocking solution for 1 hour at room temperature. Next, the brain slices were incubated in primary antibodies Rabbit anti-c-Fos (1:1000, Abcam, ab190289) overnight at 4°C . After eluting three times, the brain slices were reacted with secondary antibodies AlexaFluor-488 or AlexaFluor-555 (1:1000, Invitrogen) for 2 hours at room temperature. Then, the brain slices were eluted 3 times for 10 minutes in PBS. The images were scanned by digital pathology section system (OLYMPUS, Japan).

Neuroanatomical tract-tracing experiments

Adult anesthetized Sst-Cre mice were placed on a stereotaxic apparatus and injected AAV-DIO-RVG and AAV-DIO-EGFP-TVA into the unilateral S1Tr, followed 3 weeks later by an injection of rabies virus (RV-Enva- Δ G-mCherry) at the same site. After virus injection, we left the syringe in place for an additional 10 min and then closing the skin using surgical sutures. One week after the last injection, mice were anesthetized, perfused and removed the brain. Mice brains were sectioned into slices of 40 μ m using a freezing microtome (CM 3050S, Leica), and then put onto glass slides. The images were taken with a digital pathology section system (OLYMPUS, Japan).

QUANTIFICATION AND STATISTICAL ANALYSIS

All values were presented as mean \pm SEM. The data were analyzed by student t test, one-way ANOVA or two-way ANOVA with the post hoc as appropriate. Statistical significance was set at $p < 0.05$ (*), $p < 0.01$ (**).